Malignant Renal Tumors

10

Bahig M. Shehata, Mina M. Naguib, Jenny Lin, and Geetika Khanna

Overview and Classification

Renal tumors account for approximately 6–7 % of all pediatric cancers, with Wilms' tumor being the most common malignancy [1, 2]. Current classification and staging criteria for renal tumors, aided by advances in molecular and cytogenetic abnormalities, have allowed accurate diagnostic, staging, and therapeutic protocols [2], elucidated new categories of renal neoplasms, and created more inclusive classification (Table 10.1) [2, 3].

Overview of Imaging Features

The imaging evaluation of a suspected pediatric renal mass should always begin with ultrasound. Sonography is readily available, can be performed without sedation and intravenous contrast, and does not expose the child to ionizing radiation. If a renal mass is identified on ultrasound, further evaluation of the renal vessels and inferior vena cava (IVC) with both gray scale and color Doppler images are required to detect vascular extension, present in up to 10 % of cases [4]. Further evaluation with contrast enhanced computed tomography (CT) or magnetic resonance imaging (MRI) is also required for local staging of the mass prior to any intervention, as per the guidelines of the Children's Oncology Group (COG). Either modality can be used, depending on institutional availability and expertise [5].

In keeping with the As Low As Reasonably Achievable (ALARA) principle regarding ionizing radiation exposure, pre-contrast and multiphase contrast enhanced CT images are not required for diagnosis or staging of pediatric renal tumors [6]. A single-phase study in the portal venous phase (approximately 50 s after contrast injection) sufficiently stages a renal tumor and delineates relevant anatomy. Multiplanar CT reconstructions or multiplanar scanning with MRI can confirm the renal origin of the mass and assess its relationship to vital structures such as the renal vessels. If a partial nephrectomy is being considered, multiphase images are helpful to determine the relationship of the mass to the renal vessels and collecting system. A CT of the chest is required in all malignant renal tumors to evaluate for potential lung metastasis.

Wilm's Tumor

Definition

Wilms' tumor (*syn:* nephroblastoma), a malignant neoplasm originating from nephrogenic blastemal cells, is the second most common malignant, solid extracranial tumor in children [1, 7, 8]. It is a traditional blastematous tumor, exhibiting various stages of embryonic development and multiple lines of differentiation.

Clinical Features and Epidemiology

In children ranging from 0 to 15 years of age, Wilms' tumor occurs in seven to ten cases per million annually (1 in 10,000 children) and accounts for approximately 95 % of renal tumors, and comprises 6–7 % of all pediatric tumors [7, 9, 10]. It is the fifth most common pediatric tumor and the second most common intraabdominal tumor in children [11].

G. Khanna, M.D., M.S. (✉)
Radiology, St. Louis Children's Hospital,
Washington University School of Medicine – MIR,
510 S. Kingshighway, Box 8131, St. Louis,
MO 63110, USA
e-mail: khannag@mir.wustl.edu

B.M. Shehata • M.M. Naguib • J. Lin
Department of Pathology and Pediatrics,
Emory University School of Medicine, Pediatric Pathologist,
Children's Healthcare of Atlanta,
1405 Clifton Road, Atlanta, GA 30322, USA

D.M. Parham et al. (eds.), *Pediatric Malignancies: Pathology and Imaging*,
DOI 10.1007/978-1-4939-1729-7_10,

Table 10.1 Summary of the pediatric renal tumors described in this chapter

Classification for pediatric renal tumors
Nephroblastic tumors
Nephroblastoma (Wilms' tumor)
Favorable histology
Anaplasia (diffuse or focal)
Nephrogenic rests and nephroblastomatosis
Cystic nephroma and cystic partially differentiated nephroblastoma
Mesoblastic nephroma
Cellular
Classic
Mixed
Clear cell sarcoma
Rhabdoid tumor
Renal epithelial tumors of childhood
Translocation-associated tumors
Renal cell carcinoma associated with Xp11.2 translocations (*TFE3*)
Other translocation-associated tumors
Papillary renal cell carcinoma
Renal medullary carcinoma
Oncocytic renal neoplasms after neuroblastoma
Chromophobe renal cell carcinoma
Rare tumors
Primitive neuroectodermal tumors (PNET)
Primary rhabdomyosarcoma of the kidney
Primary synovial sarcoma

Wilms' tumor predominantly arises in young children. Greater than 80 % of Wilms' tumors are found in children younger than 5 years old, with an average age of 3.5 years [1]. Rarely, 0.16 % of Wilms' tumors are seen in neonates, and on very few occasions it occurs in adults [7].

Wilms' tumor statistics vary with respect to ethnicities. In the USA, there is a lower incidence in Hispanic/Latino compared with non-Hispanic children (RR=0.78, 95 % confidence interval=[0.64, 0.95]) [9]. The incidences in Chinese and American black children are 2.5 per million and 10.9 per million, respectively [7]. In Britain, the incidence is lower among Asian children than Caucasian children (RR=0.51, $p<0.05$) but higher among West Indian children (RR=2.55, $p<0.05$) [9].

Wilms' tumor has a slightly greater propensity to occur in girls (9.7 per million) than boys (8.4 per million). Data has shown that the age at diagnosis is significantly higher for girls than boys. The Wilms' tumor population in Europe shows similar trends with a 0.9 ratio of boys to girls (median age for girls 3 years; for boys 2 years). In Asia, a higher reported percentage of boys developed Wilms' tumor [9].

More than 90 % of Wilms' tumors present as an asymptomatic abdominal mass. Most are contained within a single lesion, 6 % present as bilateral tumors, and 12 % have multifocal disease within a single kidney. If abdominal pain (20–40 %) exists at diagnosis, there is a risk of rupture and bleeding [1, 12]. Gross hematuria (5–25 %) indicates tumor invasion into the collecting system or ureter [1, 12]. Rare cases have been reported at extrarenal sites, such as in the perirenal, inguinal, or gonadal areas, perhaps as a component of "monodermal" teratoma [8]. The average birth weight of patients with Wilms' tumors is greater than controls [7].

Symptoms present in less than 10 % of Wilms' tumor patients as a result of vascular invasion or pressure from surrounding organs. Patients with vascular invasion may present with ascites, congestive heart failure, hepatomegaly, or varicocele. Symptoms caused by tumor-induced hormones include hypertension (25 %), hypercalcemia, erythrocytosis, and von Willebrand's disease [1, 10, 12].

Ninety percent of Wilms' tumors are sporadic, and the rest occur as part of overgrowth and non-overgrowth syndromes [8]. Overgrowth syndromes include Beckwith–Wiedemann, isolated hemihypertrophy, Perlman, Sotos', and the Simpson–Golabi–Behmel syndromes. Non-overgrowth syndromes include WAGR (WT, aniridia, genitourinary anomalies, mental retardation) and Denys–Drash syndromes [1, 10]. Familial cases have an earlier age of onset and an increased incidence of bilateral disease [10].

Imaging Features

Wilms' tumor typically appears as a heterogeneous mass arising from the renal parenchyma. The normal renal parenchyma is distorted and displaced around the mass, resulting in a characteristic "claw sign" that helps confirm its renal origin [13]. On sonography, a small WT may appear uniformly isoechoic; however, more often areas of necrosis, hemorrhage, and calcification create a heterogeneous echo texture. On power Doppler evaluation, the mass typically shows decreased perfusion as compared to the normal vascular renal parenchyma. Evaluation of the renal vein with both gray scale and color Doppler evaluation is essential to exclude venous thrombus, which can be present in up to 11.3 % of WT [14]. On CT or MRI, WT typically appear heterogeneous in attenuation/signal intensity and show decreased enhancement as compared to the normal renal parenchyma (Fig. 10.1a). Intracaval extension of the tumor thrombus can be identified with a sensitivity of 84.6–96.0 % on CT (Fig. 10.1b) [15]. The presence and level of tumor thrombus in the IVC determines the surgical approach and need for preoperative chemotherapy, so the renal vein and IVC should be carefully evaluated for any filling defects. Potential pitfalls in the evaluation of the renal vein and IVC include contrast mixing artifacts and extrinsic compression of the vessels caused by a large WT.

Though microscopic extension of WT through the renal capsule is impossible to detect on imaging, gross infiltration

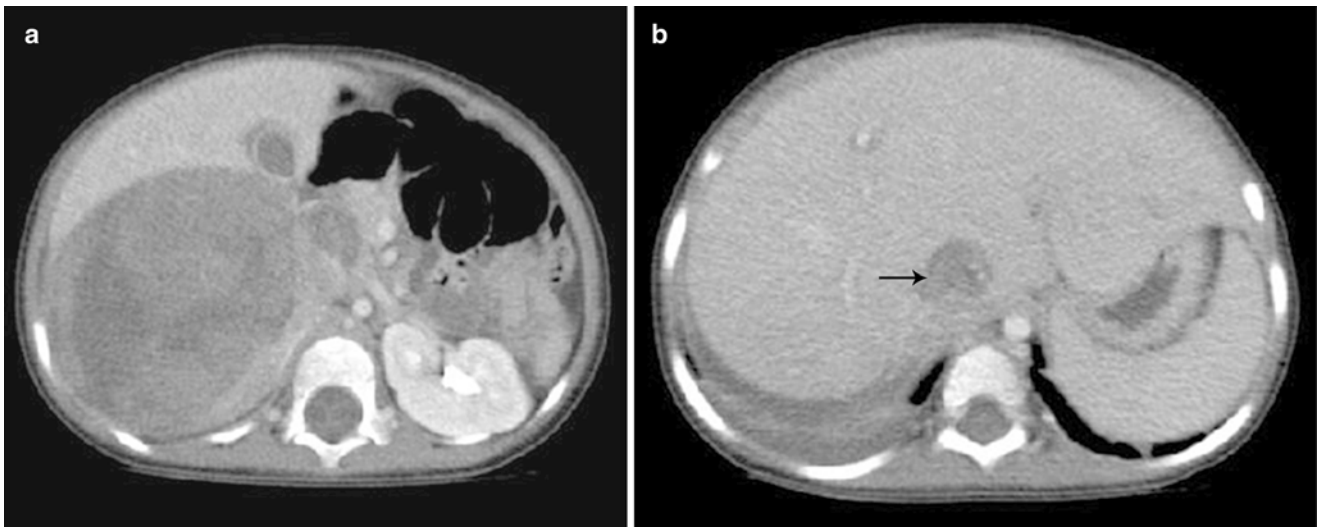

Fig. 10.1 Wilms' tumor with IVC thrombus. (**a** and **b**) Axial contrast enhanced CT images from a 4-year-old show a large heterogeneous mass in the right renal fossa with tumor thrombus distending the inferior vena cava (**b**) (*arrow*)

into adjacent structures such as the liver and psoas muscle should be evaluated on imaging. Wilms' tumor can rupture preoperatively upstaging the child to stage III with increased risk of intraabdominal recurrence. Signs of preoperative tumor rupture include ascites beyond the cul-de-sac, extracapsular perinephric fluid, and peritumoral fat stranding [16]. The regional lymph nodes, lung, and liver, common sites of metastatic disease in WT, should be carefully evaluated. Enlarged lymph nodes should be noted, though current imaging techniques have limited accuracy in detection of nodal metastasis, necessitating sampling during nephrectomy [5]. The contralateral kidney should be carefully evaluated for a contralateral WT or nephrogenic rest, as WT can be bilateral in approximately 10 % of cases [17]. Differentiation of WT from a nephrogenic rest is limited by imaging, though the former tends to inhomogeneous as compared to the homogeneous appearance of rests [18].

Pathology

Gross and Microscopic Features

The majority of Wilms' tumors form isolated, well-demarcated masses separated from the adjacent kidney (Fig. 10.2) [1, 8]. Rarely, a botryoid variant of Wilms' tumor is seen, characterized by polypoid mass occupying the renal pelvis (Fig. 10.3). After preoperative chemotherapy, significant amounts of necrosis or hemorrhage can occur. Cystic lesions require careful inspection for nodular solid areas [8].

Histology is an important prognostic indicator for Wilms' tumor. Certain histologies, particularly anaplastic Wilms' tumors, show higher risks of tumor recurrence or chemotherapy resistance [1]. Traditional Wilms' tumors contain varying amounts of three basic histological components—blastemal, epithelial, and stromal cells—which vary widely in relative proportions (Fig. 10.4) [7, 8]. If one component

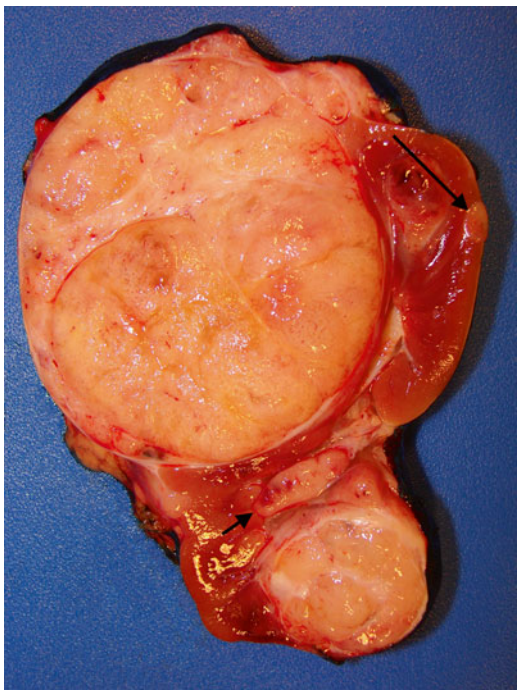

Fig. 10.2 Multifocal Wilms' tumor with renal sinus invasion (*short arrow*) and perilobar nephrogenic rest (*long arrow*)

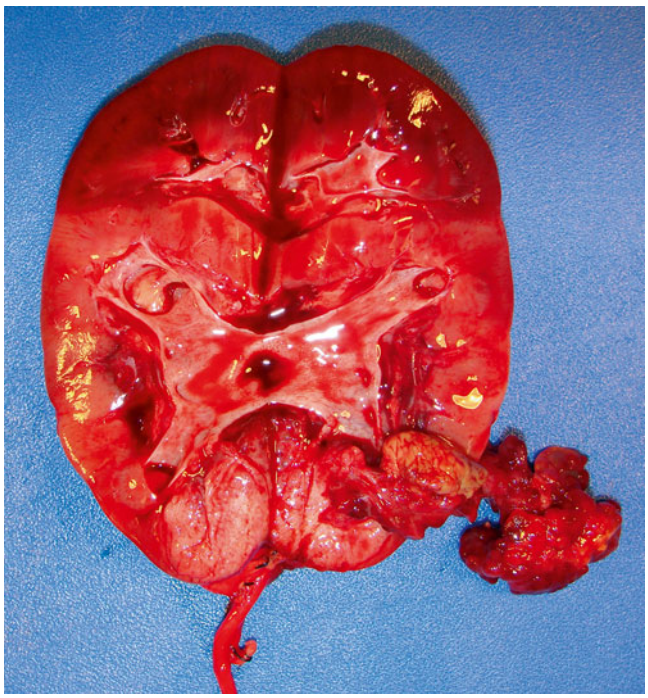

Fig. 10.3 Botryoid variant of Wilms' tumor, figure shows tumor arising in the lower pole of the kidney with a polypoid mass attached to the original tumor with a pedicle

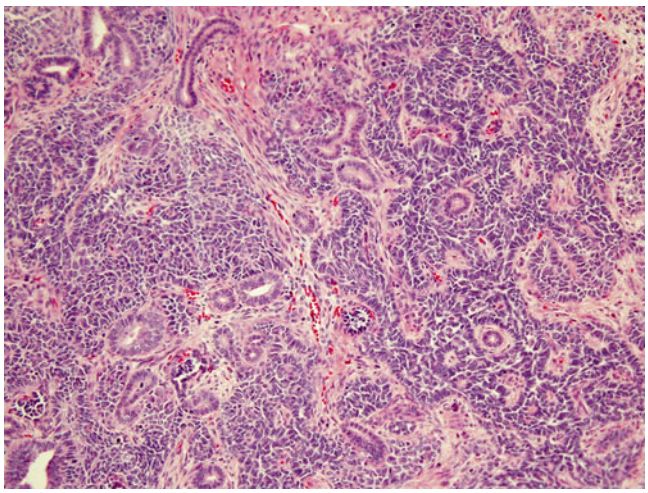

Fig. 10.4 Triphasic Wilms' showing epithelial, blastemal, and stromal components

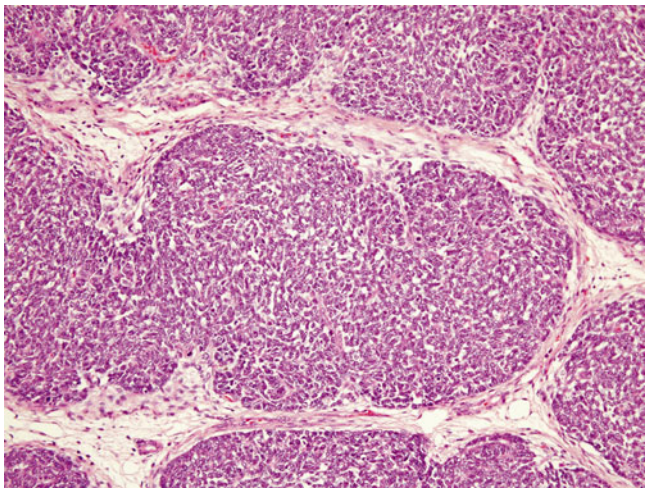

Fig. 10.5 Blastemal predominant Wilms' tumor. The tumor is composed of primitive small cells arranged in a serpentine pattern and separated by fibrovascular networks

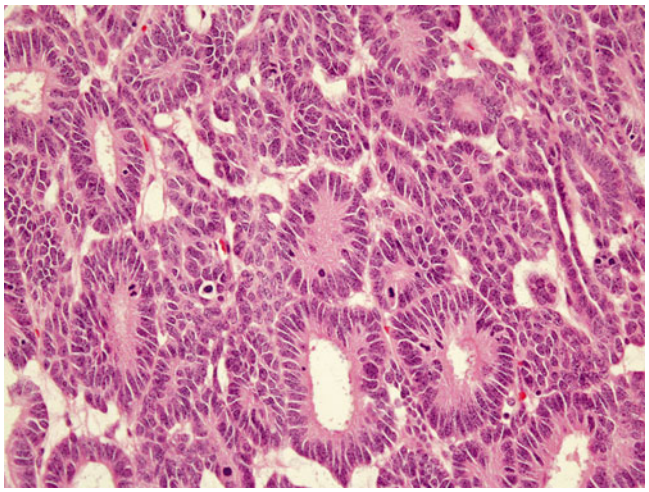

Fig. 10.6 Epithelial predominant Wilms' composed of rosette-like tubules lined by columnar epithelium with occasional mitotic figures

comprises >2/3 of a tumor, it is referred to as predominant for that specific cell type [7].

Blastemal predominant Wilms' tumors are generally more aggressive, i.e., higher stage, but usually respond to stage-specific therapy [10]. They contain sheets of small, round-to-ovoid cells with irregular nuclei, small nucleoli, and little cytoplasm, usually with mitotic figures, apoptotic bodies, and closely packed, overlapping nuclei with diffuse chromatin (Fig. 10.5) [8]. On occasion, rosette formation may resemble neuroblastoma. Growth patterns lack prognostic significance and include diffuse, serpentine, nodular, and basaloid features [7, 8].

Epithelial predominant Wilms' tumor is less aggressive but may be resistant to therapy with advanced stage [10]. It is composed of rosette-like and glomeruloid tubules lined by low columnar cells with hyperchromatic nuclei and papillary intratubular invaginations (Fig. 10.6) [7, 8]. Mucinous and squamous epithelium, neural structures, and neuroendocrine cells may also be seen [7]. With epithelial predominant Wilms' tumor, one should exclude metanephric adenoma (MA), a rare benign tumor that accounts for

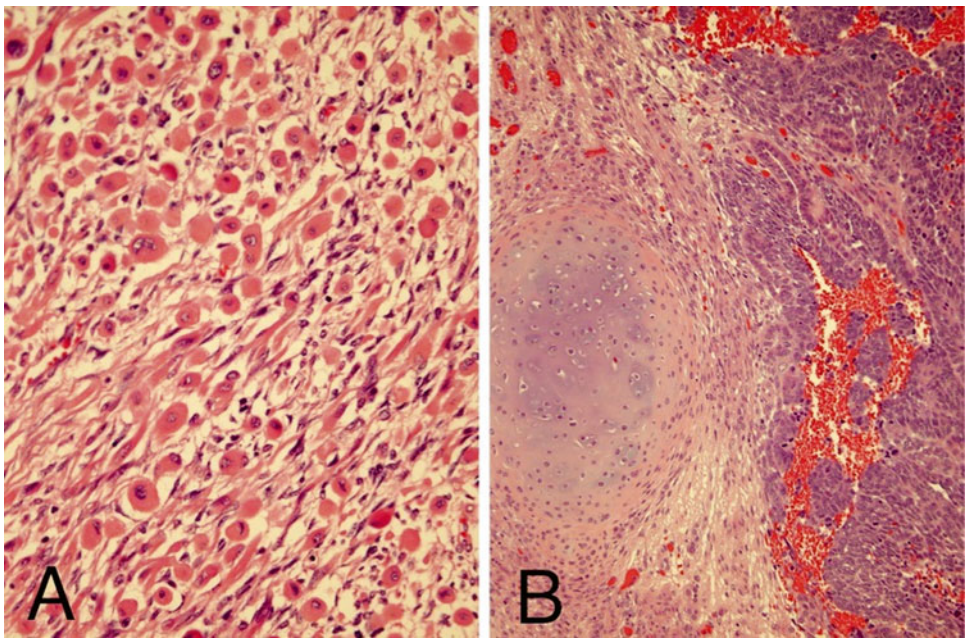

Fig. 10.7 Stromal component of Wilms' showing skeletal muscle differentiation (**a**) and cartilaginous differentiation (**b**)

~0.2–1 % of all kidney tumors [19]. MAs occur at all ages, ranging 5–80 but most commonly 40–60 years old [8, 20]. Up to 12 % of MA patients have polycythemia [21]. They are purely epithelial lesions lacking stroma and containing densely packed uniform ovoid cells with even, lymphocyte-like nuclei forming a tubular pattern, pink to clear cytoplasm and frequent psammoma bodies. Unlike Wilms' tumors, MAs contain extremely rare to absent mitoses [21], and show little or no compression of adjacent renal tissue. Metanephric adenofibromas contain both stromal and epithelial components but occur extremely rarely (only 25 cases in the NWTS series [22, 23]).

Stromal predominant Wilms' tumors, like epithelial-predominant ones, show poor clinical responses to chemotherapy [10]. They may contain hypocellular, sparse regions of immature stellate cells in a myxoid background and dense areas of primitive spindled mesenchymal cells. Other stromal cell types include smooth and striated muscle (Fig. 10.7a), adipose tissue, cartilage (Fig. 10.7b), bone, and osteoid, with muscle representing the most common differentiated stromal cell type [7, 8]. It is important in bone forming lesions to consider ossifying renal tumor of infancy, an extremely rare pediatric renal neoplasm with a benign clinical course [23]. With stromal lesions, one should also consider metanephric stromal tumor (MST), an extremely rare, entirely stromal lesion in the spectrum of metanephric neoplasms. Most MSTs occur in the first decade of life [8, 25, 26]. Characteristic concentric "onion skin" rings are observed surrounding entrapped renal tubules or blood vessels. These rings or collarettes are the most defining histological characteristic of MST.

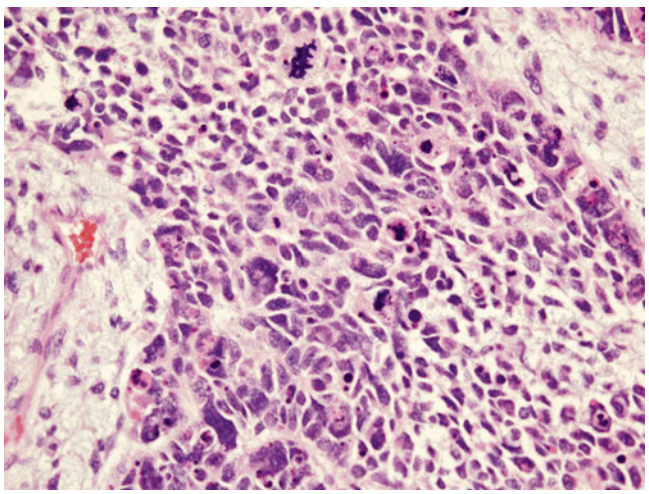

Fig. 10.8 Anaplastic Wilms' showing a multipolar mitotic figure and large anaplastic cells

Anaplasia is the major unfavorable histological variant of Wilms' tumors and accounts for 5–10 % of unilateral Wilms' tumors [1, 8, 10]. It rarely occurs in children under 2 but peaks at about 5 years of age [7, 11]. It is more common in African-American that Caucasian patients [11]. Anaplasia is defined by atypical multipolar mitotic figures, hyperchromatism, and enlarged tumor nuclei at least three times the size of adjacent ones (Fig. 10.8). Anaplasia may be focal or diffuse. With focal anaplasia, only one or two isolated intrarenal foci show anaplastic changes. Diffuse anaplasia occurs in extrarenal or multiple intrarenal locations. In stages higher than stage I, diffuse anaplasia has a significantly worse prognosis and is chemotherapy-resistant [7, 8].

Immunohistochemistry and Other Special Stains

Immunohistochemistry has a minor role in diagnosis of nephroblastomas, since the major diagnostic tool lies in tumor morphology. However, it can be helpful with needle core biopsies containing small round cell tumor. WT1, the most helpful marker, is expressed by nuclei of both blastemal and primitive epithelial cells. Primitive renal blastema also shows diffuse and strong but nonspecific positivity for CD56. Nuclear p53 expression has been reported in most anaplastic Wilms' tumors [8].

Molecular Diagnostic Features and Cytogenetics

Various genes have been implicated in hereditary and syndromic Wilms' tumor. One to 3 % of patients have a family history of inherited tumors [1, 9]. Genetically inherited cases tend to have an earlier onset and increased bilaterality [10]. Two familial genes have been specified: *FWT1* at 17q12-q21 and *FWT2* at 19q13 [10]. About 10 % of Wilms' tumor patients show associated congenital abnormalities and syndromes. Mutations of Wilms' tumor 1 (*WT1*), a tumor suppressor gene located at 11p13, occur in the Wilms' tumor, aniridia, genitourinary anomalies, mental retardation (WAGR), and Denys–Drash (DDS) syndromes (Fig. 10.9) [9]. *WT1* encodes a transcription factor important in gonadal development, ureteric budding, and nephrogenesis [1]. WAGR and DDS patients have increased risk of bilateral tumors, younger age, and renal dysfunction [10]. *WT1* mutations also occur in about 2 % of sporadic tumors [10].

Aniridia is a non-overgrowth syndrome found in 1.1 % of Wilms' tumor patients. It is caused by a defect in the *PAX6* gene located at 11p13 adjacent to *WT1*. About 40–70 % of aniridia patients have a contiguous *WT1* deletion causing Wilms' tumor [1, 10]. In addition, more than half of tumors with *WT1* mutations have coexisting ones in the beta-catenin gene (*CTNNB1*), suggesting involvement of the Wnt/beta-catenin pathway, and mutations in this gene are found in 5–15 % of Wilms' tumors overall [9, 10].

Loss of heterozygosity (LOH) of the Wilms' tumor 2 (*WT2*) gene locus located on chromosome 11p15 has been identified in up to 40 % of sporadic cases and 1–8 % of Beckwith–Wiedemann syndrome (BWS) patients [9]. BWS patients with hemihypertrophy have a 4–10 % chance of developing Wilms' tumors, 21 % of them bilateral [1, 10]. Specific genes located within the *WT2* domain include *H19* and insulin-like growth factor 2 (*IGF2*) [10]. Differential DNA methylation of these two genes reveals biallelic expression of *IGF2* in 26–77 % and hypermethylation of *H19* in 26–75 % of Wilms' tumors without LOH [9].

Wilms' tumors show LOH at chromosomes 16q and 1p in 20 % and 10 % of cases, respectively. LOH at these locations increases the risk of tumor relapse and mortality [1, 10]. Lesions that have LOH at both 16q and 1p show an even greater propensity for relapse and mortality, with the relapse-free rate dropping to 74.9 % (in combination) from 80.4 % (1p alone) and 82.5 % (16q alone) [27]. LOH at 11q occurs in 20 % of Wilms' tumors and is three to four times more common in anaplastic ones [10].

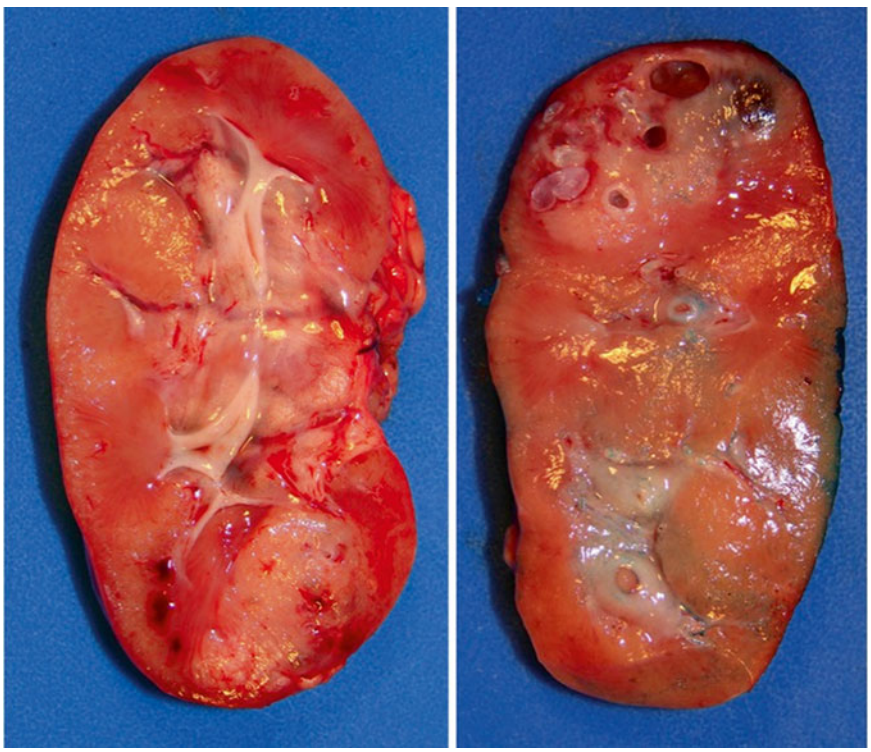

Fig. 10.9 Bilateral Wilms', nephrectomy in a patient with Denys–Drash syndrome

The Wilms' tumor gene on the X chromosome (*WTX*) on Xq11.1 is activated in up to one third of Wilms' tumors, affecting the single X in males or the active X in females as a "single hit," or monoallelic, event. *WTX* is thought to be involved in the Wnt/beta-catenin signaling pathway [1, 10].

Prognostic Features

Although survival for patients diagnosed with Wilms' tumor was once under 30 %, more than 90 % of children now have excellent outcomes [1, 11]. This marked improvement is due to adherence to protocol-based therapy that includes specific surgical approaches, enhancements in chemotherapy, and refined radiation therapy [11].

Histopathology is a major prognostic indicator, especially after preoperative chemotherapy. Blastemal Wilms' tumors are highly aggressive, and more than 75 % of this subtype present at stage III or IV. Blastema is generally responsive to chemotherapy but is associated with a high relapse rate [7, 10]. Substantial reduction in size subsequent to chemotherapy is a good prognostic indicator [7], but persistent viability after chemotherapy of a blastemal lesion indicates a poor prognosis [8]. Diffusely anaplastic tumors are resistant to chemotherapy but with complete excision have better prognosis [1]. Epithelial predominant tumors are less aggressive, and more than 80 % present at stage I. Although more resistant to chemotherapy, epithelial and stromal-predominant subtypes have a good prognosis after complete resection [1, 7].

Wilms' tumor metastasizes most commonly to the lungs and less commonly to the liver. About 12 % of patients show hematogenous metastases at diagnosis, 80 % extending to the lungs. Lymph node involvement indicates distant metastases but is difficult to assess [1, 7, 8, 11]. About 20 % of favorable histology tumors relapse after therapy [11], but patients are usually curable if there is no liver or mediastinal metastasis. However, repeated relapses indicate a very poor prognosis [7].

LOH for chromosomes 1p and 16q in stage I and II Wilms' tumors confers a significantly worse prognosis and is now used to stratify Wilms' tumor patients into different levels of risk and treatment [11].

Nephrogenic Rests and Nephroblastomatosis

Nephrogenic rests (NRs), abnormally persistent clusters of embryonal renal parenchyma tissue beyond 36 weeks of gestation, are known precursors of Wilms' tumors (WT) [28–30]. Multifocal or diffuse lesions are called nephroblastomatosis. Based on their topographic location with respect to the renal lobe, nephrogenic rests are separated into perilobar nephrogenic rests (PLNR), found at the periphery of the lobe (often subcapsular), and intralobar nephrogenic rests (ILNR), present anywhere within the kidney [8, 31, 32]. Both of these subtypes can be further classified as dormant, sclerosing, hyperplastic, or neoplastic (development into WT), depending on their eventual fate [29–32].

Nephrogenic rests are often clinically asymptomatic and are usually discovered incidentally in conjunction with Wilms' tumor [30]. Higher than average birth weight significantly correlates with NR diagnosis, especially PLNR. A small percentage of patients with NRs have associated syndromes or genetic abnormalities. WAGR and Denys–Drash syndromes are strongly associated with ILNR, along with other genital anomalies like hypospadias and cryptorchidism. Overgrowth syndromes like BWS and hemihypertrophy (HH) have a higher prevalence of PLNR but a slight correlation with ILNR. PLNRs also occur in Perlman syndrome, and trisomies 13 and 18 [29, 33].

The subtypes and various fates of NRs can be histologically distinguished based on their location, gross features, and morphologic appearance. Perilobar nephrogenic rests are predominantly composed of well circumscribed blastemal tissue (Fig. 10.2; long arrow), while ILNRs are primarily composed of stromal or epithelial tissue with irregular margins that often interdigitate with surrounding normal interstitial tissue. PLNRs usually present with multiple lesions that well demarcated from adjacent kidney, while ILNRs mostly occur as isolated or few foci that often blend with adjacent kidney [7, 30].

The pathogenesis of NRs is undoubtedly linked to that of Wilms' tumor, with perhaps over ten genes involved. Many studies have reported similar LOH in both NRs and adjacent Wilms' tumors [34–37]. Since PLNR is positioned in the periphery of the renal lobe, their genetic dysregulation likely occurs later in development than ILNR, following lobar pattern establishment. The deeper location of ILNR within the renal lobe supports an earlier developmental abnormality [29].

Imaging Features of Nephrogenic Rests

Recent advancements in imaging technology have greatly facilitated the detection of small renal tumors and nephrogenic rests. Both contrast enhanced CT and contrast enhanced MRI can detect nephrogenic rests as small as 4–5 mm, so routine intraoperative exploration of the contralateral kidney is no longer recommended [38].

Because US is widely available and relatively inexpensive, it is the primary imaging method for screening patients at risk of nephrogenic rests. On US, NR lesions are typically homogeneous and hypoechoic or isoechoic to normal kidney tissue. As nephrogenic rests are relatively less vascular than normal renal parenchyma, use of power Doppler imaging can aid in the detection of nephrogenic rests. Ultrasonography

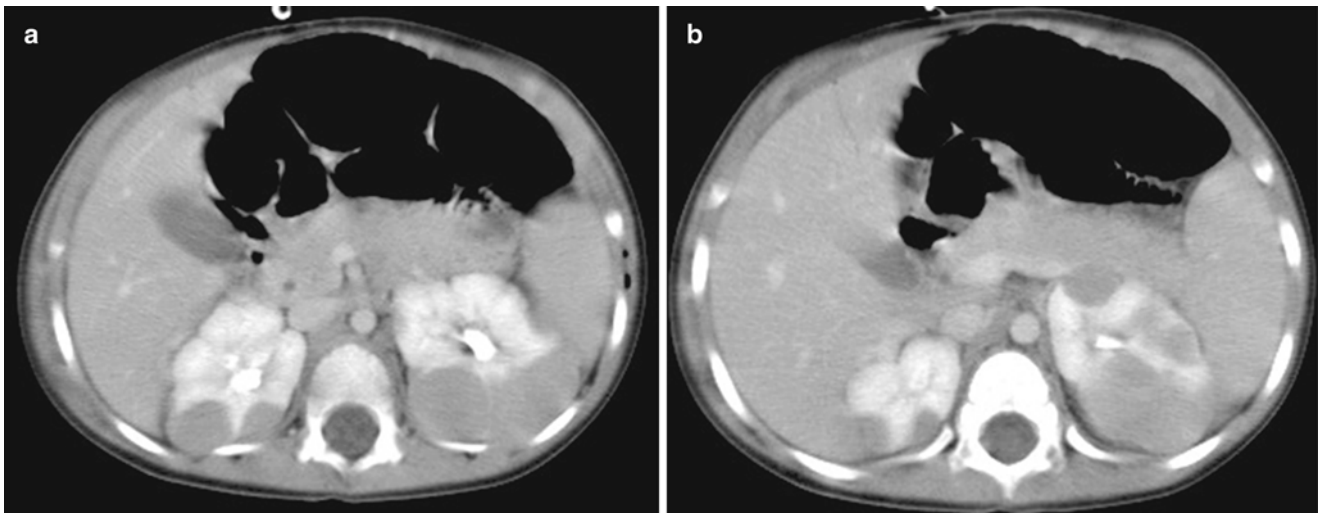

Fig. 10.10 Bilateral Wilms' tumor (nephroblastomatosis). (**a** and **b**) Axial contrast enhanced CT images of the abdomen in a 3-year-old show bilateral hypodense lesions consistent with nephroblastomatosis

can detect NR as small as 8 mm, but has a lower sensitivity than CT or MRI [18, 39, 40]. On CT, nephrogenic rests are most evident on post contrast images as homogeneous lesions that enhance less than the normal renal parenchyma. On MR, hyperplastic rests are relatively T2 hyperintense compared to normal renal parenchyma, while sclerotic rests are relatively hypointense on T2 weighted images [39]. As on CT, nephrogenic rests enhance less than normal renal parenchyma on post contrast MR images.

Imaging differentiation of nephrogenic rests from Wilms' tumor can be difficult. While nephrogenic rests tend to have a more homogeneous appearance on all imaging modalities, heterogeneity favors Wilms' tumor. Both tumor and hyperplastic rests tend to be bright on T2-weighted images [39]. The size of the lesion per se is not reliable for differentiation, as nephrogenic rests up to 5 cm in diameter have been reported [18].

The presence of multiple bilateral nephrogenic rests is referred to as nephroblastomatosis (Fig. 10.10a, b) [41]. A specific subtype of nephroblastomatosis is diffuse hyperplastic perilobar nephroblastomatosis (DHPLN), characterized by a rind of nephroblastic tissue surrounding the renal parenchyma (Fig. 10.11). On imaging the kidneys are diffusely enlarged but maintain their normal reniform shape. The nephroblastic rind is confined to the periphery of the kidney, has homogeneous attenuation/signal intensity, and enhances less than the normal kidney.

Nephroblastomatosis should be distinguished from renal lymphoma, which can also result in bilateral renal masses. Children with nephroblastomatosis are younger (<5 years of age) and lack the extensive retroperitoneal lymphadenopathy usually seen in patients with lymphomatous involvement of the kidneys.

Fig. 10.11 Diffuse nephroblastomatosis showing overgrowth of perilobar nephroblastic tissue

Cystic Nephroma and Cystic Partially Differentiated Nephroblastoma

Cystic nephroma (CN) and cystic partially differentiated nephroblastoma (CPDN) are two uncommon benign renal tumors macroscopically characterized by multilocular cysts. The two entities are well demarcated from the rest of the kidney and have no solid components except for septa composed of fibrous tissue. A distinction is drawn between CN and CPDN in that the former contains only mature septal elements such as tubules while the latter contains embryonal elements or blastema in the cyst walls [7, 8].

For CN and CPDN, there exist four criteria that characterize the lesion. First, the entity is composed entirely of cysts and their septa. The lesion is discrete from the surrounding

renal parenchyma and well demarcated. The septa are the only solid component of the tumor and completely encase the cysts without any solid expanding nodules. Finally, the cysts are lined by flattened, cuboidal, or hobnail epithelium [42].

Cystic nephroma is distinguished by its fibrous septa that is well differentiated and contains only mature elements such as tubules. Also, mature tissue such as heterologous skeletal muscle can also be seen in CN.

Cystic partially differentiated nephroblastoma macroscopically and microscopically resembles CN but contains various immature septal elements. Usually this difference is characterized by poorly differentiated blastemal cells in the septa that may contain other embryonal cell types such as stroma or epithelia comprising poorly differentiated glomeruli, cartilage, fibrous tissue, mesenchyme, fat, tubules, or striated muscle intermixed with blastemal cells [42].

CPDN shows no excessive mitotic activity or evidence of contiguous extension or vascular involvement. The "partially differentiated" term is derived from the mixture of undifferentiated blastemal tissue with partially or well-differentiated renal tissue [43]. Cystic nephroma does not present with this spectrum of differentiation.

CN is benign,as tumor-related death or metastasis has not been previously reported. Local recurrence of the lesion after resection has been reported, most probably due to outgrowth from residual tissue and not malignancy [44].

Cystic partially differentiated nephroblastomas have an equally favorable prognosis with 100 % survival in some studies. This applies to stage 1 and 2 CPDN, which are both successfully treated with complete resection of the tumor and varying amounts of chemotherapy [45]. However, one study has reported two cases in which CPDNs undertook a more aggressive course and lead to death [43]. The more aggressive potential of CPDN may be due to the malignant potential of the poorly differentiated tissue present in the septa. The extremely favorable prognosis of CN and CPDN provides additional separation from Wilms' tumor, which has a less favorable prognosis.

Imaging Features of Cystic Tumors

Cystic nephroma and cystic partially differentiated nephroblastoma are relatively uncommon benign lesions that are indistinguishable on imaging [46]. They are typically solitary, multilocular lesions sharply demarcated from an otherwise normal remaining kidney. The masses are usually large, averaging 8–10 cm in size, and involve only part of the kidney. These are multicystic lesions, and with no solid nodules, that may protrude into the renal pelvis/ureter. On sonography, the mass consists of multiple anechoic cystic areas separated by septations (Fig. 10.12a, b). These cystic areas can vary in size from microscopic to 4 cm in diameter. The microcystic areas may mimic solid areas due to the closely packed septations. On CT and MRI, CN and CPDN typically appear as well circumscribed, multicystic masses that have variable enhancement of septations on the post contrast images. The septations are typically hypointense on precontrast T1 and T2 weighted images due to fibrous tissue in them. The differential diagnosis of a multilocular cystic renal mass in a child includes cystic Wilms' tumor or renal cell carcinoma; clear cell sarcoma; cystic variants of mesoblastic nephroma; and segmental

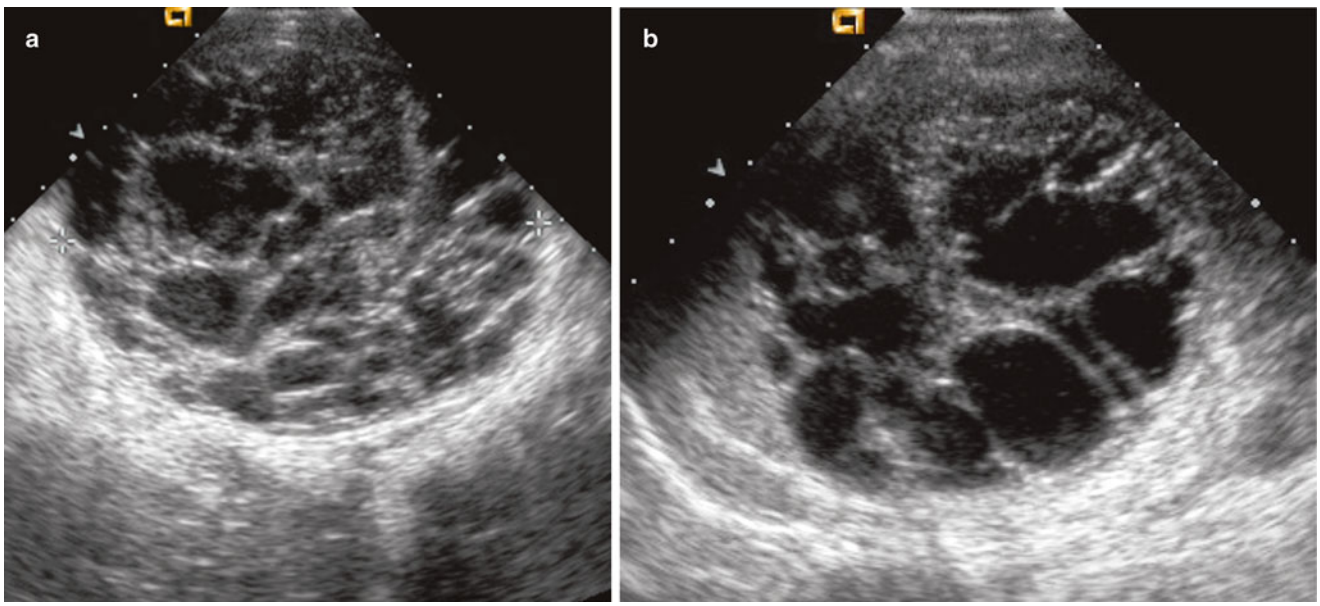

Fig. 10.12 Multilocular cystic nephroma. (**a** and **b**) Sonographic images from a 9 month old show a multiloculated cystic mass arising from the left kidney. No solid components are noted. Pathology confirmed a multilocular cystic nephroma

forms of multicystic dysplastic kidney. The presence of solid components within a cystic mass should make one consider a diagnosis other cystic nephroma/cystic partially differentiated nephroblastoma. If a cystic pulmonary lesion is identified in a child with a multicystic renal mass, this should lead one to consider a DICER 1 mutation with cystic nephroma and coexistent pleuropulmonary blastoma [47].

Mesoblastic Nephroma

Definition

Mesoblastic nephroma (MN), also known as congenital mesoblastic nephroma (CMN), is a mesenchymal rare renal neoplasm most commonly diagnosed prenatally or in early infancy. This spindle cell neoplasm can be classified as either classic or cellular or mixed pattern [7, 8].

Clinical Features and Epidemiology

Incidence and Prevalence

Although CMN only represents less than 5 % of all pediatric renal neoplasms, it is the most common congenital renal tumor, with over 90 % of patients diagnosed before age 1 and almost no patients presenting after the age of 3. The cellular variant represents approximately 40–60 % of CMN, with the classical and mixed subtypes constituting the remaining percentage with about an equal prevalence [8, 48].

Population Features

The majority of renal tumors diagnosed within the first 6 months of life are CMN, so it must be included in the differential diagnosis of any infant with a renal mass. Because its incidence drops off significantly after early childhood, diagnosis of any spindle cell tumor as CMN must be questioned in patients older than 3 years. There does not appear to be any definitive gender predisposition, but some studies report a slight male prevalence [49, 50]. The general median age of diagnosis is approximately 20–35 days, with the cellular type (median: 3–4 months) being diagnosed at a significantly older age than the classic (median: 7 days) or mixed (median: 2 months) variants [49, 50].

Presenting Symptoms and Signs

Most patients present with an asymptomatic abdominal mass discovered upon physical examination or after imaging analysis. Other symptoms include abdominal swelling and protrusion, abdominal pain, hypertension, hypercalcemia, and hematuria [48, 50, 51]. These tumors may cause polyhydramnios during pregnancy, requiring preterm delivery in a reported 71 % of CMN associated fetuses [48].

Imaging Features

Mesoblastic nephroma presents as a solitary unilateral mass with variable cystic/solid mass in the neonate, typically within the first 3 months of life [52]. Mesoblastic nephroma has been detected in utero on prenatal sonography as a heterogeneous renal mass as early as 26 weeks. These masses can be associated with polyhydramnios and premature labor [53]. The classic and cellular subtypes of CMN differ in their imaging appearances. Classic CMN presents as a uniform soft tissue mass with minimal, predominantly peripheral, enhancement seen on post contrast CT or MRI. However, the cellular variant of CMN can have a more heterogeneous appearance and can vary from a predominantly cystic to mixed solid and cystic mass (Fig. 10.13a, b). Areas of cystic change, necrosis, and hemorrhage can be seen on all imaging modalities in cellular CMN, corresponding to its pathologic appearance.

Pathology

Gross and Microscopic Features

Grossly, the tumor is usually solid but rarely can have a prominent cystic appearance. Congenital mesoblastic nephroma tend to be firm pale to tan-colored lesions (Fig. 10.14), with the cellular variant being softer and more likely to demonstrate necrosis or hemorrhage than the classic variant. The mixed subtype shows both characteristics. The tumor often infiltrates normal adjacent renal parenchyma and perinephric fat. As previously mentioned, the cellular type is usually much larger in volume than the mixed or classic types [7, 8, 48].

Histologically, classic CMN demonstrates morphology similar to that of uterine leiomyoma and infantile fibromatosis; it contains bundled spindle cells, infrequent mitosis, and absence of necrosis (Fig. 10.15a). The spindle cells lie within collagenous stroma, show an interlacing fascicular pattern, and infiltrate surrounding renal parenchyma as finger-like projections. The cellular variant has a more malignant appearance, with an increased nuclear: cytoplasmic ratio, cellularity, and mitotic index and significantly more necrosis and hemorrhage (Fig. 10.15b). CMNs lack the blastemal components observed in Wilms' tumor and do not demonstrate characteristic vascular patterns, nuclear grooves, or clear cells as seen in clear cell sarcoma of the kidney [8, 51, 52]. However, they often entrap renal tubular elements, which may show atypia.

Immunohistochemistry and Other Special Stains

The most common immunohistochemical characteristic of CMN is diffuse nonspecific reactivity for vimentin and focal reactivity for smooth muscle actin [8, 51]. The tumor usually

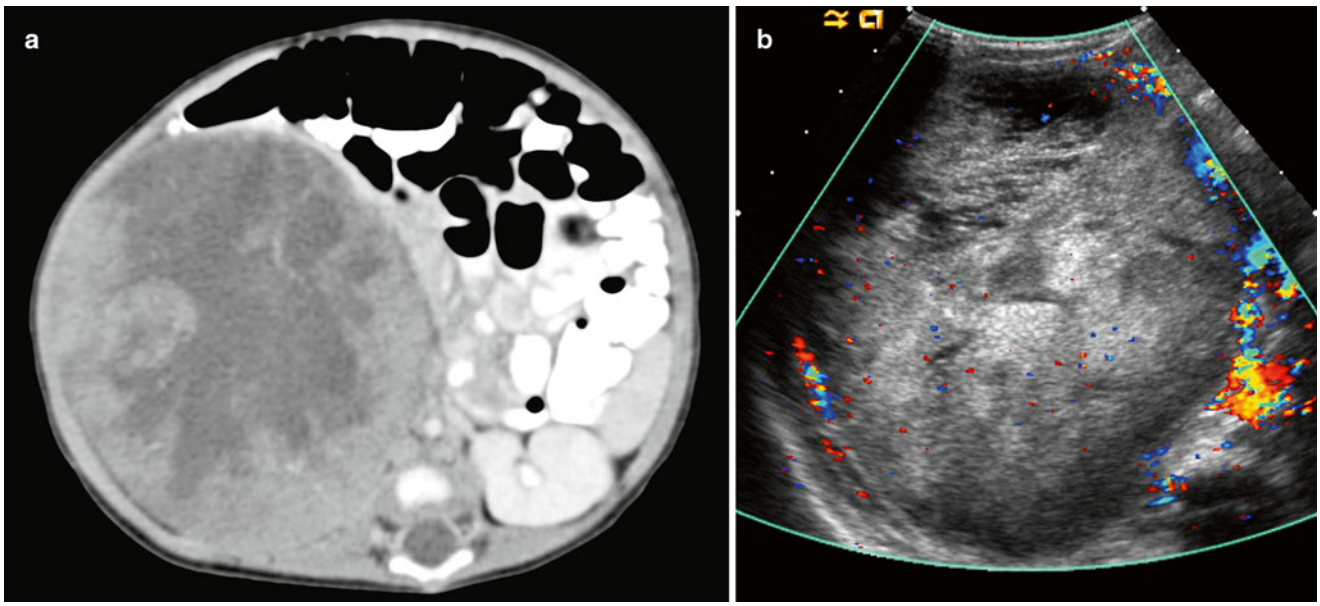

Fig. 10.13 Mesoblastic nephroma. Axial contrast enhanced CT (**a**) and color Doppler image (**b**) from a 54 day old neonate shows a heterogeneous, well circumscribed mass consistent with a cellular variant of mesoblastic nephroma

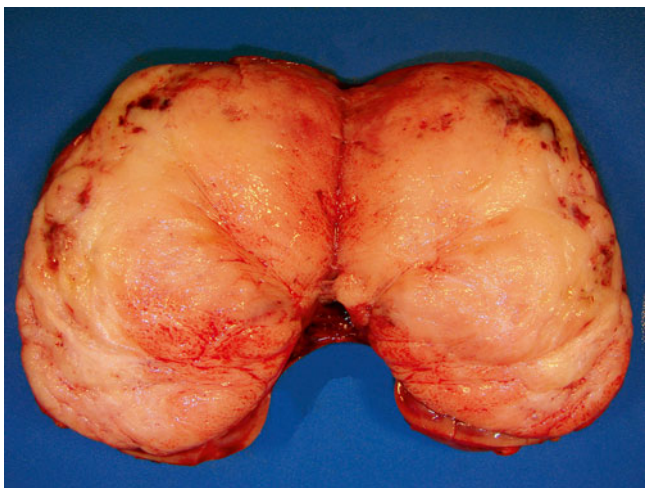

Fig. 10.14 Congenital mesoblastic nephroma showing firm, pale-colored cut surface with small cystic and hemorrhagic areas

does not show immunoreactivity for desmin, S-100, cytokeratin, AE1/AE3, epithelial membrane antigen, bcl-2, or CD99 [51, 54].

Molecular Diagnostic Features and Cytogenetics

Recent cytogenetic studies have found strong genetic correlations between the cellular variant of CMN and congenital infantile fibrosarcoma (CFS). Using RT-PCR and fluorescence in situ hybridization, a study found that five out of six cellular CMN tumors and five out of five CFS tumors tested were found with the same t(12;15)(p13;q25) translocation that resulted in a *ETV6-NTRK3* (aka *TEL-NTRK3*) gene fusion [55]. Both of these entities have also been associated with genetic polysomies at chromosomes 8, 11, 17, and 20 [55, 56], with trisomy 11 being strongly correlated with CMN. Because cellular CMN and CFS have similar histological and morphologic features and the same genetic abnormalities, these two neoplasms appear to represent the same entity, with cellular CMN being the renal variant. Additionally, it has been reported that primary bronchopulmonary fibrosarcoma (BPFS), a rare lower respiratory neoplasm affecting children and young adults, also carries the t(12;15) *ETV6-NTRK3* genetic abnormality [55, 57]. Thus, we consider CMN and BPFS as visceral variants of CFS. The same t(12;15) *ETV6-NTRK3* fusion does not appear with classic CMN, which may be found in conjunction with cellular CMN in the mixed subtype. *ETV6-NTRK3* fusion is also found in a dissimilar tumor, secretory carcinoma of the breast [55].

Prognostic Features

Mesoblastic nephroma is usually a benign neoplasm with overall good prognosis after nephrectomy. Local recurrences and metastasis to the brain, lungs, heart, bone, and liver have been reported, with the majority of these relapses being associated with the cellular variant of CMN. Overall, about 10 % of CMN tumors relapse and such recurrences almost always

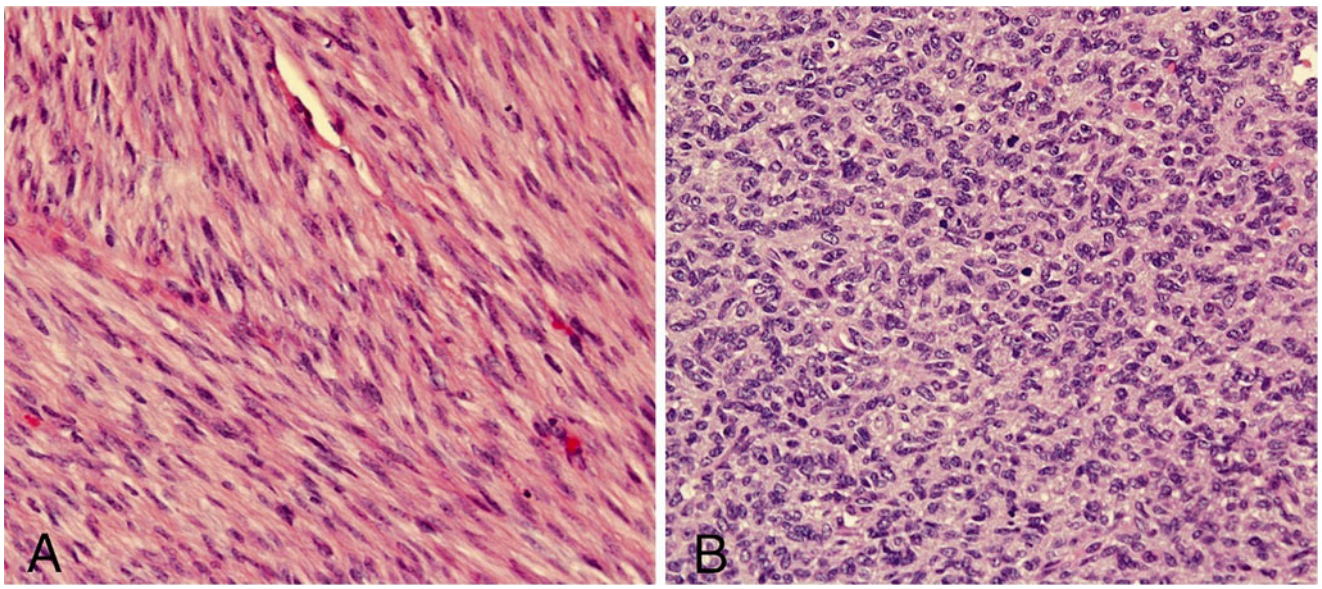

Fig. 10.15 (**a**) Classic CMN showing interlacing fascicular pattern of benign spindle cells. (**b**) Cellular variant showing sheets of round cells with increased nuclear cytoplasmic ratio and abundant mitotic figures

occur during the first year after initial diagnosis [48]. The survival overall is very high at >95 %. Late stage cellular CMN occurring in patients older than 3 years carries the worst prognosis. Adjuvant chemotherapy is not recommended after complete resection [7, 49].

Clear Cell Sarcoma of the Kidney

Definition

Clear cell sarcoma of the kidney (CCSK) is rare renal pediatric neoplasm with a generally unfavorable prognosis [58, 59]. Because of its greater tendency towards bone metastasis, the tumor has been called bone metastasizing renal tumor of childhood, and it has also been referred to as sarcomatous Wilms' tumor [7].

Clinical Features and Epidemiology

CCSK is extremely rare; only 20 new cases are reported annually in the USA [60]. Overall accounts for 3–5 % of all pediatric renal neoplasms. Nevertheless, CCSK still represents the second most common childhood renal tumor [61].

CCSK patients present at a mean age of 36 months; most are diagnosed between ages 2 and 3 years, with a large decline in incidence afterwards [60]. It is extremely uncommon during the first 6 months of life and has seldom been reported in adolescents and adults [59, 60]. Patients have a male predominance with an average ratio of 2:1 [7, 59, 60].

Clinical manifestations of CCSK include an abdominal mass or swelling, abdominal pain, constipation, decreased appetite, fever, gross hematuria, hypertension, and vomiting [59, 63]. Approximately 5 % present with metastasis, with the lymph nodes being the most common site [8, 60]. According to the National Wilms' Tumor Study (NWTS), approximately 26 % of CCSK cases present at stage I, 35 % at stage II, 34 % at stage III, and 5 % at stage IV, with negligible numbers at stage V [59, 60].

Imaging Features

Clear cell sarcoma typically presents as a large, solid but inhomogeneous renal mass with cystic/necrotic areas, that on imaging is indistinguishable from WT [64]. Foci of calcification can be present in up to 25 % of cases. This aggressive tumor can have extracapsular spread and vascular extension at the time of initial presentation, though the latter is less common than in WT cases. The most common sites of metastasis are bone, lymph nodes, lung, and liver.

Pathology

Gross and Microscopic Features

Grossly, CCSKs are large, soft, and gray-tan to white in appearance. They are uniform, fleshy, well circumscribed,

sharply demarcated, and almost always present unilaterally in the kidneys. Tumors are usually solid but may be focally cystic with necrosis and hemorrhage [7, 8, 54, 63]. The tumors often involve renal medulla and may replace and distort the entire kidney [7, 59]. Renal vein invasion occurs in approximately 5 % of cases [59, 60]. Tumors measure between 2.3 and 24 cm [60].

Perhaps the most diagnostically difficult aspect of CCSK is its histological variability: nine variations have been described [59, 60]. The classic pattern contains cords or nests of ovoid, epithelioid, and spindle shaped cells separated by consistently spaced fibrovascular septa [67, 60]. These septa characteristically feature branching or "chicken-wire" capillaries that vary in width. Tumor nuclei are uniform in shape, and their cytoplasm is clear to pale with an ill-defined cell border (Fig. 10.16) [60, 63]. Although over 90 % of CCSK predominately or focally demonstrate the classic pattern, most also present one of the other eight identified histologic variants, percentages: myxoid (50 %), sclerosing (35 %), cellular (26 %), epithelioid (13 %), palisading (11 %), spindle cell (7 %), storiform (4 %), and anaplastic (2.6 %) [60]. The different patterns are essentially varying alterations of the cord/nest or septal cell appearance, and they therefore cannot be separated as distinct biological entities.

Immunohistochemistry and Other Special Stains

Clear cell sarcoma of the kidney can only be definitely diagnosed by microscopic analysis Immunohistochemistry has limited usefulness in excluding other renal neoplasms. Almost all CCSKs are nonspecifically immunoreactive for vimentin [59, 60]. Positive expression has also been associated with NGFR, muscle specific actin, bcl-2, alpha-1-antitrypsin, and CD56 [7, 8, 54, 59, 60]. CCSKs are negative for cytokeratin, CD99, S100, desmin, WT1, von Willebrand factor, epithelial membrane antigen, CD688, and NSE [7, 59, 60, 63].

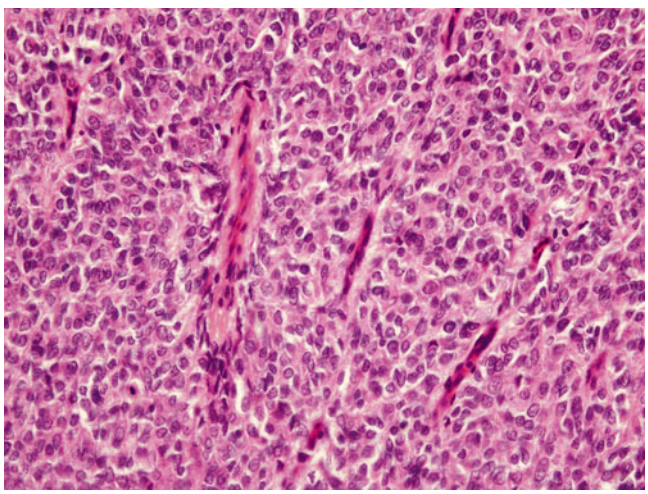

Fig. 10.16 Clear cell sarcoma, classic pattern showing cords of ovoid epithelioid cells separated by fibrovascular septa

Molecular Diagnostic Features and Cytogenetics

Various genetic abnormalities are associated with CCSK, but no common consensus has been established as to its probable underlying molecular pathogenesis. Among the most common genetic defects reported is a t(10;17)(q22;p13) that may be associated with *TP53* [58, 65]. *TP53* expression occurs with anaplastic CCSK [60], but, *TP53* mutations have not been consistently implicated among the other subtypes. One study found a rearrangement of chromosome 17 (*YWHAE*) and 10 (*FAM22*) that resulted in an *YWHAE-FAM22* transcript in some CCSK [65]. Other reports note t(1;6)(p32.3;q21) and t(2;22).

The most common loss or gain mutations in CCSK include a 1q gain and a 19p loss, with 16p loss, 10q loss, 4p loss, and 10q gain being less common [59, 65].

Studies have reported loss of imprinting in insulin-like growth factor 2 (IGF2) in CCSK comparable to Wilms' tumor [66]. One study reported an up-regulation of neural markers with simultaneous activation of Sonic hedgehog and phosphoinositide-3-kinase/Akt pathways [61].

CCSK has not been associated with genetic syndromes or familial inheritance.

Prognostic Features

Traditionally, a renal neoplasm with unfavorable prognostic outlook, recent advancements in treatment have greatly improved the overall survival of CCSK to about 70 % [63]. The addition of doxorubicin chemotherapy to existing treatment regiments greatly improved the outcome contributing to a 98 % survival rate among those diagnosed at stage 1 and an increase in the survival stage 2 or 3 patients from 30 to 70 % [60], with decreased bone metastasis to about 20 % [7]. Patient age is an important prognostic factor, with those being diagnosed at less than 2 years or greater than 4 years of age (outside of the 2–4 age median) having a lower survival rate. Tumor necrosis has been linked to lower survival rates [50].

The likelihood of relapse after initial CCSK treatment is approximately 20–40 %, with the most common sites of relapse being bone, lung, brain, and abdomen [59]. CCSK has a propensity to metastasize longer after nephrectomy than Wilms' tumor (median time 24 months), so that patient monitoring is required for longer periods of time [60].

Malignant Rhabdoid Tumor of the Kidney

Definition

Malignant rhabdoid tumor of the Kidney (RTK) is one of the most lethal pediatric neoplasms and the most lethal childhood renal tumor [67, 68]. This tumor is extremely rare and arises primarily in children less than 2 years of age. It is characterized by mutation of the *INI1* gene.

Clinical Features and Epidemiology

Rhabdoid tumor of the kidney is an extremely rare pediatric neoplasm, accounting for only about 2 % of all renal tumors in the National Wilms' Tumor Study (NWTS) [7, 68].

This neoplasm occurs almost exclusively in young children, with about 80 % of cases occurring in patients younger than 2 years of age and 95 % of cases in patients less than 3 years [2, 7]. Almost no cases are reported in children over the age of 5 [8]. The average age at presentation is approximately 17 months with a male predominance of 2:1 [68].

Children with RTK present with an abdominal mass sometimes accompanied by painful swelling, hematuria, fever, hypertension, hypercalcemia, and elevated serum levels of parathormone activity [67–70]. The majority of cases exhibit metastatic spread at the time of diagnosis, with only about 15 % of patients presenting at stage 1 or 2 (tumor limited to the kidney and not extending beyond renal capsule). The most common sites of metastasis include the lungs, abdomen, liver, brain and bone [68].

Imaging Features

Rhabdoid tumor of the kidney is a highly malignant neoplasm which presents as a large, centrally located, heterogeneous soft-tissue mass involving the renal hilum. The margins of this aggressive tumor tend to be indistinct, as opposed to WT which can form a pseudocapsule around it. It has been suggested that the presence of a subcapsular fluid collection, lobulated contour of the mass, and linear areas of calcification between the lobules should raise suspicion for a rhabdoid tumor of the kidney [71, 72]. However, these are nonspecific findings which can be seen with more common renal tumors such as WT as well. The diagnosis of a rhabdoid tumor should be considered in a young child (typically <2–3 years of age), with an aggressive appearing renal tumor. MRI of the brain is recommended in all children with rhabdoid tumor of the kidney due to the known association with synchronous or metachronous central nervous system rhabdoid tumors and the risk of brain metastasis. Other reported sites of metastasis include lung, liver, and heart [73].

Pathology

Gross and Microscopic Features

Grossly, RTKs present as large masses almost entirely replacing the kidney, with an average weight of 389 g and tumor diameter of 9.6 cm [68]. The surface of the lesion is soft, solid, and gray-pink to tan in color, often with extensive necrosis and hemorrhage [8, 68, 70]. Tumors are usually unencapsulated and show vascular invasion and infiltration into the renal parenchyma. Most of the lesions are unilateral; bilateral involvement almost always results from metastasis [68].

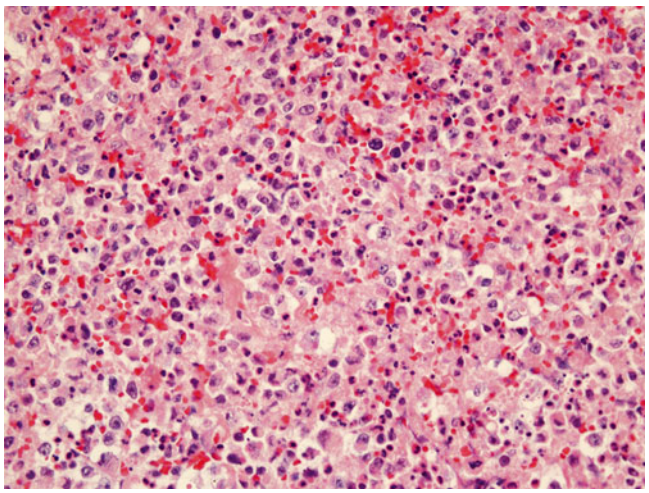

Fig. 10.17 Rhabdoid tumor, classical type composed of monomorphous noncohesive sheets of tumor cells showing vesicular nuclei, and prominent nucleoli. Note: tumor necrosis and hemorrhage

Histologically, the majority of RTK neoplasms present with "classical" morphology, but variations exist [68]. The classical type is characterized by noncohesive sheets of tumor cells showing vesicular nuclei, prominent nucleoli, and abundant eosinophilic cytoplasm containing large oval hyaline inclusions (Fig. 10.17) [7, 8, 68]. However, the presence of cytoplasmic inclusions is variable. Nuclear pleomorphism is moderate and, mitoses are numerous. Other morphologic patterns include sclerosing, epithelioid, spindled, lymphomatoid, vascular, pseudopapillary, and cystic variations [68]. The presence of multiple intratumoral patterns is not uncommon, as no single pattern (including classical) composes more than 65 % of the lesion in most cases. Transitions between patterns are often gradual, but some lesions show abrupt changes similar to collision tumors [68].

Immunohistochemistry

RTK shows strong immunopositivity for vimentin in the cytoplasmic inclusions as well as in the cytoplasm [68]. INI1 immunoreactivity is characteristically absent in the nucleus of RTK tumor cells, with such reactivity being demonstrated in the cells of almost all other pediatric renal neoplasms except for medullary carcinoma [8]. Other occasionally positive markers include alpha-1-antichymotrypsin, desmin, epithelial membrane antigen, myoglobin, neurofilaments, neuron-specific enolase, and S100 protein [7].

Molecular Diagnostic Features and Cytogenetics

Rhabdoid tumors can occur in various extra-renal sites including soft-tissue and the central nervous system. The common genetic abnormality among all rhabdoid tumors is the mutation and downregulation of the *SMARCB1/hSNF5/*

INI-1 gene found at chromosome 22q11 [74]. *SMARCB1* is a tumor suppressor gene that encodes for the SMARCB1 protein, a subunit in the SWI/SNF chromatin remolding complex that has been implicated in various processes including neural development, transcriptional regulation, and cell-cycle regulation [75]. SMARCB1 protein interaction with other proteins is implicated in many RTK pathways.

Abnormalities in genes associated with normal neural development, such as *DOCK4*, *PTN*, *PTPRK*, and *SPOCK1* [76], are commonly found in RTK of *B1*. SMARCB1 protein is necessary for normal neural development, and it interacts with proteins such as pleiotrophin (encoded by PTN), which regulates differentiation and proliferation of neural stem cells. Other neural differentiation pathways, such as the Notch pathway, are compromised in RTs, leading to the hypothesis that these neoplasms may arise in neural progenitor cells with arrested development [76].

Normal expression of *SMARCB1* plays an important role in transcriptional regulation. An intact SWI/SNF complex regulates gene expression by disrupting DNA-histone interactions and allowing transcriptional proteins (activating or repressing) more efficient access to their targets. SMARCB1 hypothetically links SWI/SNF with transcriptional regulators [76]. Proteins known to physically interact with SMARCB1 include ATP1B1, FZD7, and PTN, all of which are implicated in RT development [74, 76]. SMARCB1 also interacts with trithorax and polycomb protein families, implicated in transcriptional activation and repression respectively [76]. The balance between the two families is mediated by a direct interaction between SMARCB1 and MLL1 protein, a member in the trithorax family. MLL1 protein facilitates transcriptional activation by methylation of histone H3 lysine 4 (H3K4), while the polycomb family is responsible for transcriptional repression through methylation of histone H3 lysine 27 (H3K27). With the disruption of this interaction, the trithorax family is unable to adequately activate transcription levels resulting in an overall transcriptional repression from the polycomb family.

A marked downregulation of cyclin-dependent kinase inhibitors *CDKN1A* and/or *CDKN2A* due to a loss of interaction with *SMARCB1* gene products occurs in RTs [76]. Without this kinase inhibition, RT cells more readily proliferate. Genes implicated in tumor invasion and metastasis are also upregulated in RTs; these include *MMP12*, *NCOA3*, *RSU1*, *SPP1*, *TRFC*, and *ZNF217*. Conversely, genes associated with tumor suppression, such as *COL18A1*, *DOCK4*, *PTPRK*, and *SELENBP*, are downregulated in RTs [76].

Prognostic Features

Rhabdoid tumor of the kidney has an extremely poor prognosis, with an overall survival rate of about 23 % [76]. More than 70 % of patients present with metastasis, and over 80 % demonstrate metastatic spread within 3–4 months after diagnosis [7, 76]. Tumor stage at diagnosis is strongly correlated to survival, with the vast majority of survivors presenting at stage I or II [7]. Despite intensive chemotherapy, the survival rate has not increased, and RTK remains resistant to most forms of medicinal therapy. One study, however, has reported the successful use of ICE (isofamide, carboplatin, and etoposide) and VDCy (vincristine, doxorubicin, and cyclophosphamide) in the treatment of a stage IV RTK [70]. This patient remained recurrence free for 24 months after treatment. A higher survival rate is found among females (56.3 %) as compared to males (11.1 %) [68].

Pediatric Renal Cell Carcinoma

Definition and Overview

Pediatric renal cell carcinomas (PRCC) are rare neoplasms accounting for approximately 2–5 % of all childhood renal tumors [77, 78]. These entities although sharing the same name generally differ from adult renal cell carcinoma in their histology and cytogenetic characteristics. Conventional or pure clear cell carcinoma of the kidney (accounting for about 70–80 % of adult RCC neoplasms) is extremely uncommon in children, comprising about 6–20 % of PRCC and almost never carrying the characteristic chromosome arm 3p abnormality found in adults [79, 80]. The more common subtypes of childhood RCC include translocation-associated neoplasms (20–40 %) and papillary PRCC (30 %) [77]. Renal medullary carcinoma (RMC) associated with sickle cell trait and oncocytic RCC associated with post-neuroblastoma treatment have been described but are extremely rare. These four are described separately below. Additionally, about 25 % of PRCCs differ histologically from the aforementioned subtypes and are classified as PRCC NOS [77].

Generally, PRCC has a reported median age of anywhere from 9 to 17 years, differentiating these lesions from most other pediatric renal neoplasms, which occur earlier in life [78]. No racial or gender predominance has been consistently reported, although some indicated higher prevalence in African-Americans and in females. Unlike adult RCC, in which lesions are often found incidentally, patients with PRCC usually present with symptoms including protruding abdominal mass, abdominal pain, fever, hematuria, and weight loss, with only about 10 % presenting asymptomatically [8, 78]. Additionally, children with PRCC are more likely to be found with locally advanced disease at diagnosis as compared with adults [78]. Also, a significant number of PRCC patients present in the context of underlying syndromes such as von Hippel–Lindau disease and tuberous sclerosis or have been previously treated with chemotherapy

for another pediatric neoplasm [70]. Each subtype carries unique cytogenetic characteristics detailed below. Overall, the 5-year survival rate is approximately 30–90 % depending on the subtype and staging. Patients with lymph node (LN) metastasis (about 30 % of cases) have about a 90 % survival rate, but the rate drops to 10–15 % in cases with non-localized/non-nodal metastasis [80]. As with other pediatric lesions, PRCCs are generally treated by radical nephrectomy, with surgical impact on overall prognosis depending on disease stage [80]. Additionally, the effectiveness adjunct retroperitoneal lymphadenectomy in addition to radical nephrectomy is controversial [81, 82]. Targeted therapies have become the standard in adult RCC treatment, while the role of such therapies has not been established in children.

Translocation-Associated PRCC

Translocation-associated PRCC forms a distinct group of neoplasms occurring almost exclusively in children and adolescents. The most common translocations involve the *TFE3* gene on chromosome Xp11.2 and less commonly the *TFEB* gene on chromosome 6p21 [77, 80]. Genetic abnormalities in the *TFE3* gene can result in multiple gene fusion products, with the *ASPL-TFE3* fusion (found also in alveolar soft-part sarcoma) involving chromosome 17 [t(X;17)(p11.2;q25)] and the *PRCC-TFE3* fusion involving chromosome 1 [t(X;1p11.2;q21)] being the two most common types [77]. Other less common fusions involving this gene include *CLTC-TFE3* [t(X;17)(p11.2;q23)], *PSF-TFE3* [t(X;1)(p11.2;p34)], and *NONO-TFE3* [inv(X)(p11;q12)] [83–85]. These fusions result in increased expression of TFE3 protein [8]. *TFE3* and *TFEB* genes belong to the microphthalmia transcription factor (MiTF) family implicated in helix-loop-helix leucine zipper transcriptional function [80].

Additionally, these neoplasms can rarely occur in children who received prior chemotherapy with presentation onset ranging from 4 to 13 years after treatment. Such a correlation may be due to treatment with DNA topoisomerase II inhibitors and/or alkylating agents that may facilitate chromosomal instability [80].

Grossly, translocation associated PRCCs are usually unifocal, circumscribed neoplasms, with a tan-yellow appearance and hemorrhage and necrosis (Fig. 10.18) [77, 78]. Multifocal PRCCs are rare and usually occur in the context of other underlying syndromes including von Hippel–Lindau disease and tuberous sclerosis [77].

Generally, the microscopic features of translocation PRCCs are consistent regardless of the variant (Fig. 10.19). Papillary morphology is common with many clear cells [8, 79]. Cells are arranged in nests, tubules, and papillae with clear to markedly granular eosinophilic cytoplasm [8, 77]. The cells have distinct infiltrative borders, with entrapment of renal tubules and vascular invasion commonly observed. Prominent nucleoli and psammoma bodies are commonly present in these neoplasms [78, 84, 85]. Some trends have emerged correlating to specific translocation variants but are not consistently reliable. For example, the *ASPL-TFE3* variant tends to have more abundant cytoplasm, psammoma body formation, and prominent nucleoli than *PRCC-TFE3*, while the latter tends to present with less calcification and be more nested and compactly arranged [8, 77].

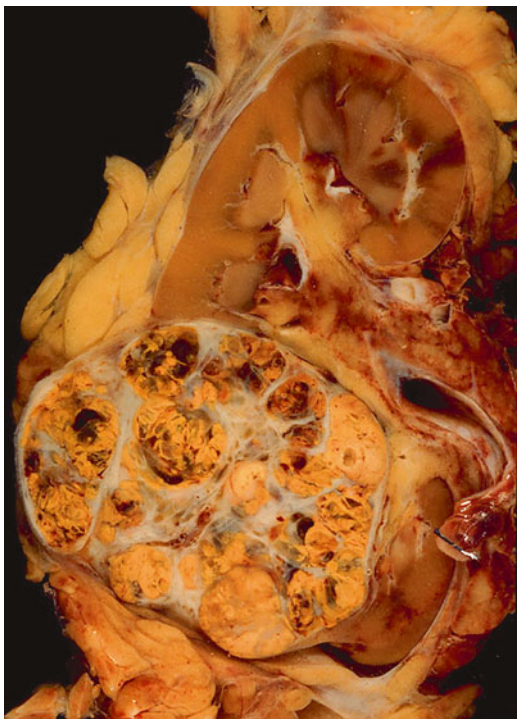

Fig. 10.18 Renal cell carcinoma showing a circumscribed neoplasm with a tan-yellow appearance, hemorrhage, and necrosis

Immunohistochemistry is important in the diagnosis of PRCCs, because a significant amount cannot be easily distinguished from other PRCC variants and even other pediatric renal neoplasms. Nuclear expression for TFE3 protein is both sensitive and specific in diagnosing all types of this PRCC variant [77]. Translocation associated PRCCs differ from adult RCC in that the former rarely stains for vimentin and various epithelial markers such as AE1/AE3, Cam 5.2, cytokeratin 7, and EMA [77, 80]. Additionally, cathepsin-K positivity has been reported [80]. Like adult RCC, translocation PRCCs stain for CD10, AMACR, and RCC antigen, while being negative for CD117. *TFEB*-RCCs can be further distinguished from other variants in that they show positivity for melanocytic markers HMB-45 and Melan-A.

The overall prognosis of translocation PRCCs is unclear with some studies reporting favorable outcome even with LN metastasis while others indicating a poor prognosis regardless of stage at presentation. However, distant metastasis is generally associated with poor prognosis, with further tumor progression being seen in 45 % of these cases [77]. The

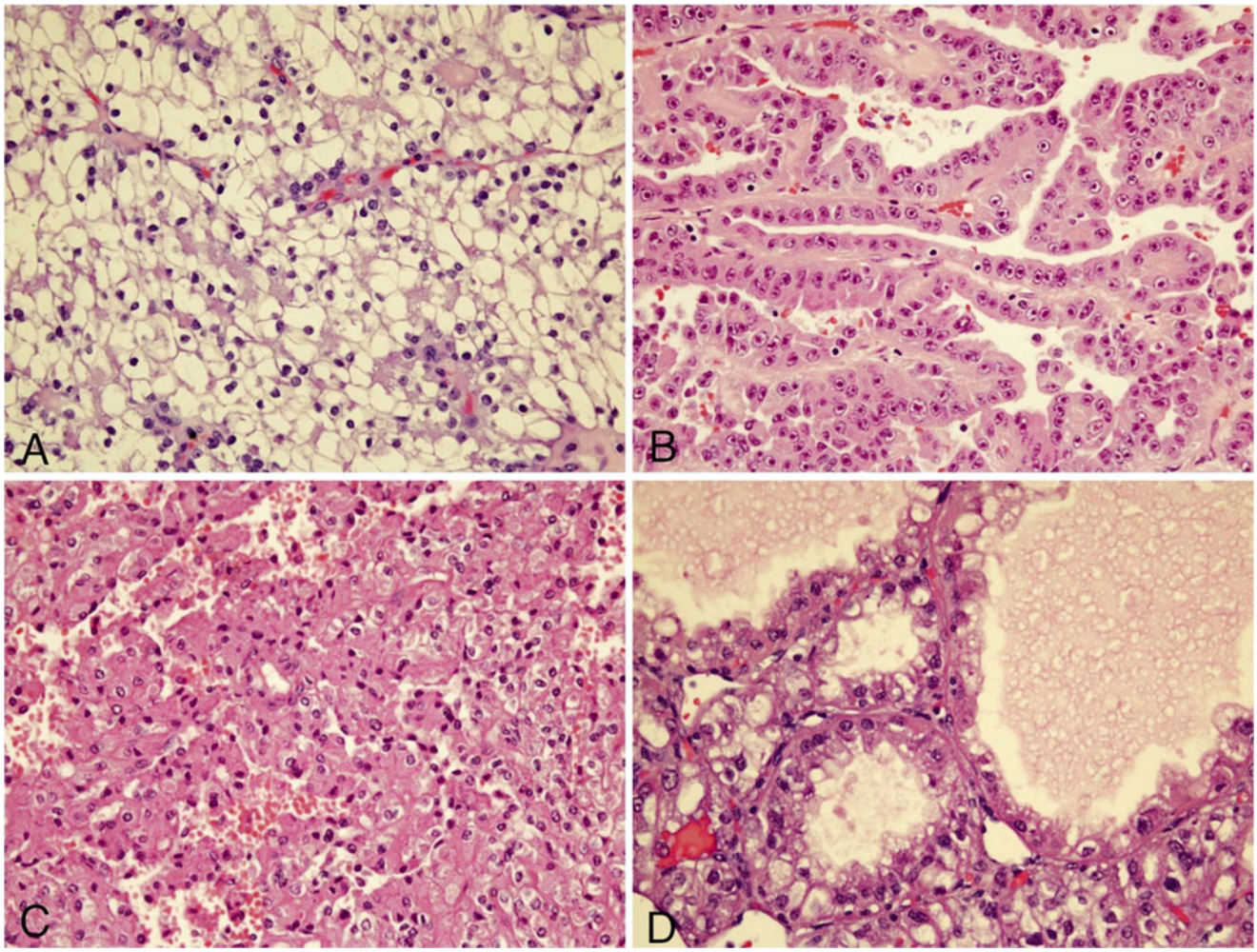

Fig. 10.19 Clear cell carcinoma, various patterns: sheets of clear cells showing well-defined cell borders (**a**), papillary configuration (**b**), showing granular eosinophilic cytoplasm (**c**), and papillary pattern with intracytoplasmic acidophilic inclusion (**d**)

TFEB variant has been reported to have a less aggressive clinical course compared with TFE3 [8]. Aside from radical or partial nephrectomy, the optimal treatment for these lesions remains undetermined. The use of antiangiogenics and targeted therapies has been reported with limited success [87–89].

Papillary PRCC

Papillary PRCC is the second most common subtype of PRCC and accounts for approximately 30 % of all cases [77]. This neoplasm is further separated into two groups, type 1 and type 2. Many patients with this lesion present in the context of preexisting tumors, which include metanephric adenoma, metanephric adenofibroma, and Wilms' tumor [77].

Papillary RCC has a similar gross presentation to translocation associated PRCCs, occurring unifocally and having circumscribed borders [77]. It has a tan yellow appearance and may be hemorrhagic [90]. Type 2 lesions tend to be larger (mean: 5.6 cm) than type 1 (mean 3.8 cm) and are also more likely to show extracapsular invasion [91].

Microscopically, cells of papillary PRCCs are arranged in papillary and tubular configurations and often contain foamy macrophages [77]. Specifically, type 1 lesions are characterized by cuboidal cells with scant cytoplasm arranged in a single layer, while type 2 lesions have a higher nuclear grade with more eosinophilic cytoplasm and are characterized by pseudostratification. These neoplasms are usually encapsulated but penetration of the surrounding fibrous pseudocapsule is not uncommon. Both subtypes of papillary PRCC can be difficult to diagnose, as type 1 has considerable histological overlap with metanephric adenoma and well-differentiated Wilms' tumor and type 2 is histologically similar to t(X;1)(p11.2;q21)-associated PRCC [77].

Immunohistochemistry can be helpful in differentiating papillary PRCC from histologically similar neoplasms.

Cytokeratin 7 is positive in 87 % of type 1 lesions and 20 % of type 2 lesions, while EMA usually stains for both types [92]. Additionally, this lesion is negative for WT1. Since epithelial differentiated Wilms' tumor and metanephric adenoma are only limitedly positive for cytokeratin 7 and EMA and positive for WT1, these stains can help separate type 1 lesions from these other neoplasms. Also, papillary PRCC is often positive for vimentin, which can be helpful in differentiating type 2 from translocation associated PRCC [77].

The genetic etiology of papillary PRCC is poorly understood, with very little being reported specifically about the pediatric variant. In the adult population, however, these lesions have multiple chromosomal aberrations, with a tendency to form trisomies [91]. Type 1 lesions show strong tendency for abnormalities in chromosome 19 while type 2 shows frequent abnormalities in chromosomes 5, 6, 8, 10, 11, 15, 18, and 22.

Like other PRCCs, the papillary variant's prognosis depends on stage at presentation. Type 2 lesions appear to have an overall more aggressive clinical course with a higher incidence of venous invasion, LN metastasis, and distant metastasis [91].

Imaging Features

Renal cell carcinoma is usually smaller in size than WT at presentation with an average size around 6 cm [93]. CT and MRI reveal a nonspecific solid intrarenal mass which enhances less than the normal kidney. Heterogeneous areas of necrosis and hemorrhage maybe present. Intratumoral calcification is seen more frequently with PRCC than with WT. Lymph node metastasis are common at the time of presentation and can be seen even with small primary tumor (Fig. 10.20a, b). Approximately 40 % of patients have lymph node or distant metastatic disease at presentation, with the most common sites of distant metastasis being lung, liver, and bone [94].

Renal Medullary Carcinoma

Renal medullary carcinoma (RMC) is an extremely rare pediatric neoplasm arising from collecting duct epithelium, associated with sickle cell trait, and characterized by a highly aggressive clinical course. Sickle cell trait is present in about 8 % of African Americans but the incidence of RMC within this population is unknown [95]. Over 80 % of RMC cases occur in African Americans with an almost 2:1 ratio of males to females. Age range at presentation is 5–51 years [96, 97]. There is a 3:1 predilection for involvement in the right kidney [97]. Patients may present with flank pain, hematuria, and abdominal mass [95, 98–100]. Widespread metastasis is extremely common at presentation.

Grossly, a poorly circumscribed tumor extensively infiltrates the renal medulla and protrudes into the renal hilum [77]. Lesions are tan to gray, firm, and lobulated, with areas of necrosis and hemorrhage common (Fig. 10.21) [101]. Tumors have an average diameter of 7.4 cm (range: 1.9–18 cm) and are not predominantly cystic. Due to its aggressive infiltration, it is often difficult to determine the original or dominant mass [77].

Microscopically, RMCs are characterized as high-grade epithelioid cells with large nuclei and prominent nucleoli. The cells are arranged in a cribriform and tubular architecture with acidophilic cytoplasm and show prominent stromal desmoplasia and neutrophils (Fig. 10.22) [77]. Other common features include the presence of chronic inflammatory infiltrate, drepanocytes, and abundant eosinophilic cytoplasm [77, 97]. This lesion shows similar histological characteristics

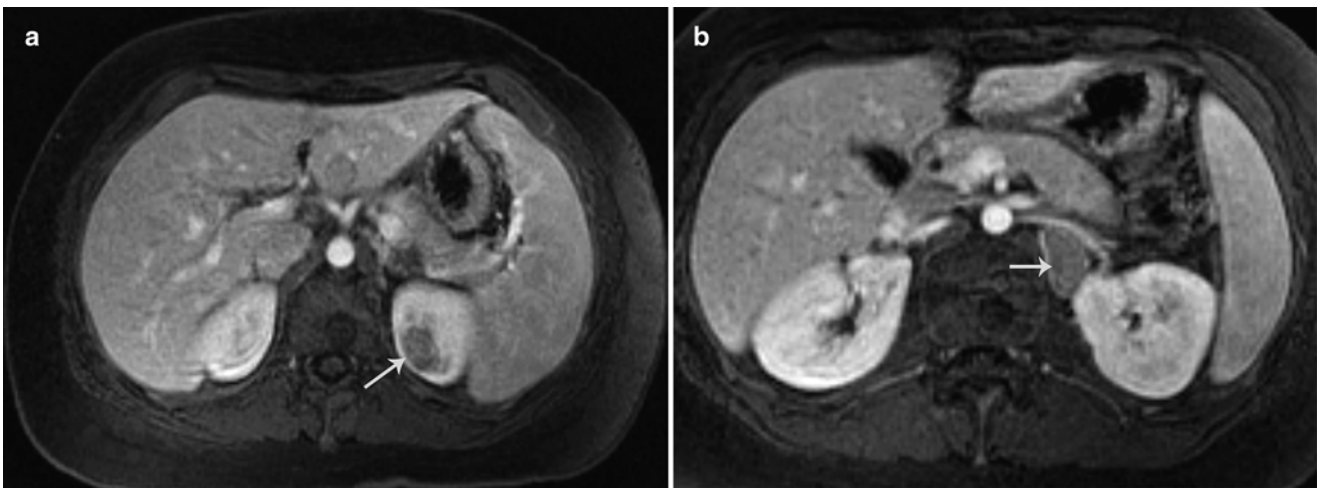

Fig. 10.20 Renal cell carcinoma. Axial post contrast MR images from a 15-year-old girl show a small renal mass at the upper pole of the right kidney (*arrow*) (**a**) and enlarged retroperitoneal lymph nodes (*arrow*) (**b**)

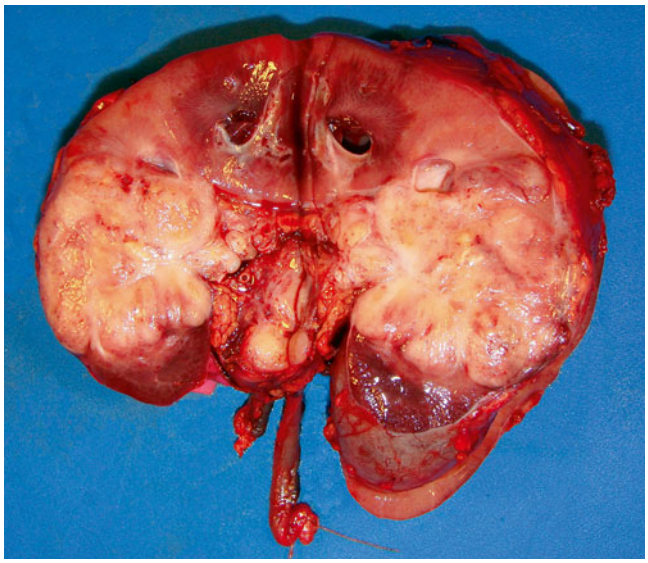

Fig. 10.21 Renal medullary carcinoma occupying the medullary portion of the kidney and extending to the hilum

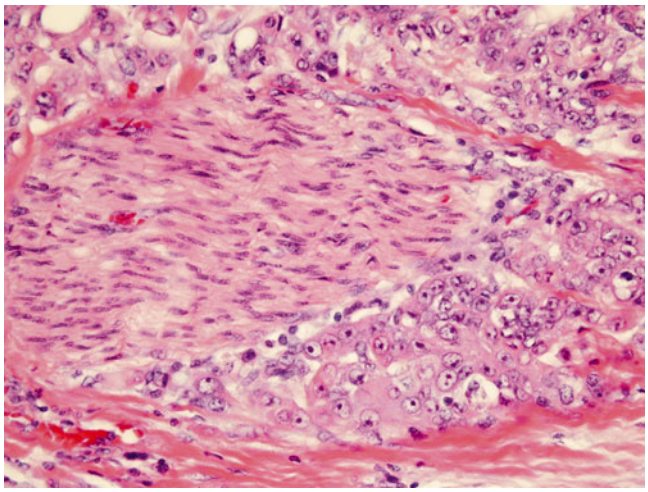

Fig. 10.22 Microscopically showing high-grade epithelioid cells mimicking rhabdoid tumor. Tumors cells show perineural invasion

to rhabdoid tumor, having similar loss of nuclear INI-1 protein positivity [97].

Immunohistochemistry is usually not needed to diagnose RMC, which expresses AE1/AE3 and EMA and does not stain for high molecular weight cytokeratin. RMC is variably positive for cytokeratin 7, CAM 5.2, and vimentin [77, 97].

No common genetic abnormalities have been reported with some studies even failing to detect losses or gains [97]. Balanced translocations reported include t(3;8)(p21;q24), t(9;22)(q34;q11), and t(10;16)(q22;q22). Monosomy for chromosome 11 has been reported, with the betaglobin gene being located on 11p [98, 102].

Prognosis is extremely poor in this neoplasm, with mortality reaching 100 % (1, 8). Approximately 50 % present at stage IV, and survival is reported beyond 16 months post diagnosis (mean: 4 months) [96, 97]. Treatment with carboplatin, paclitaxel, and high-dose-intensity MVAC chemotherapy has been reported to extend survival to up to 16 months post diagnosis [96].

Imaging Features

Renal medullary carcinoma is an aggressive malignancy, with poor prognosis that typically presents with advanced disease at presentation. A specific diagnosis of renal medullary carcinoma can be suggested on imaging due to its unique demographic features (teenagers/young adults with sickle cell trait) and characteristic imaging findings (Fig. 10.23a, b) [103]. These include a poorly circumscribed, infiltrative, hypodense mass located centrally within the kidney. Renal sinus invasion is characteristic and the infiltrative mass can result in reniform enlargement of the kidney with peripheral satellite nodules. The mass has a heterogeneous appearance due to areas of internal necrosis and hemorrhage. The right kidney is involved in approximately 70 % of renal medullary carcinoma. Regional lymphadenopathy is common at presentation. Common sites of metastatic disease include the lung, liver, pleura, and omentum [104].

Oncocytic PRCC Following Neuroblastoma

Oncocytic PRCC is an extremely rare pediatric neoplasm associated with previous neuroblastoma diagnosis. It is thought that this entity arises due to the potentially carcinogenic effects of chemotherapy and/or radiotherapy treatment [105]. However, some patients have received no chemotherapy for neuroblastoma yet still presented with oncocytic PRCC. Thus, an underlying genetic relationship between the two neoplasms may be the cause. Among the small pool of reported patients, age at neuroblastoma presentation ranged from 4 to 24 months, with subsequent oncocytic PRCC diagnosis occurring at an average of about 7–10 years post-neuroblastoma [105, 106]. Among the reported cases, a slight female predilection is noted [105].

Grossly, these lesions tend to be multifocal and occur bilaterally. Tumor size ranges from 3.5 to 8 cm (mean: 5.1 cm) [77, 105].

Microscopically, cells in oncocytic PRCC are solid and occasionally papillary in arrangement, containing abundant eosinophilic cytoplasm [77]. Cells also show oncocytoid features and cellular heterogeneity with high nuclear grade. Cell and nuclear size and shape can vary greatly, with some cells showing reticular cytoplasm [105].

Oncocytic PRCC usually does not require immunohistochemistry for diagnosis, but the lesion has been reported to be positive cytokeratins 8, 18, and 20, EMA, and vimentin, and it is negative for S-100, HMB45, and cytokeratins 7, 14, and 19.9 [77, 105].

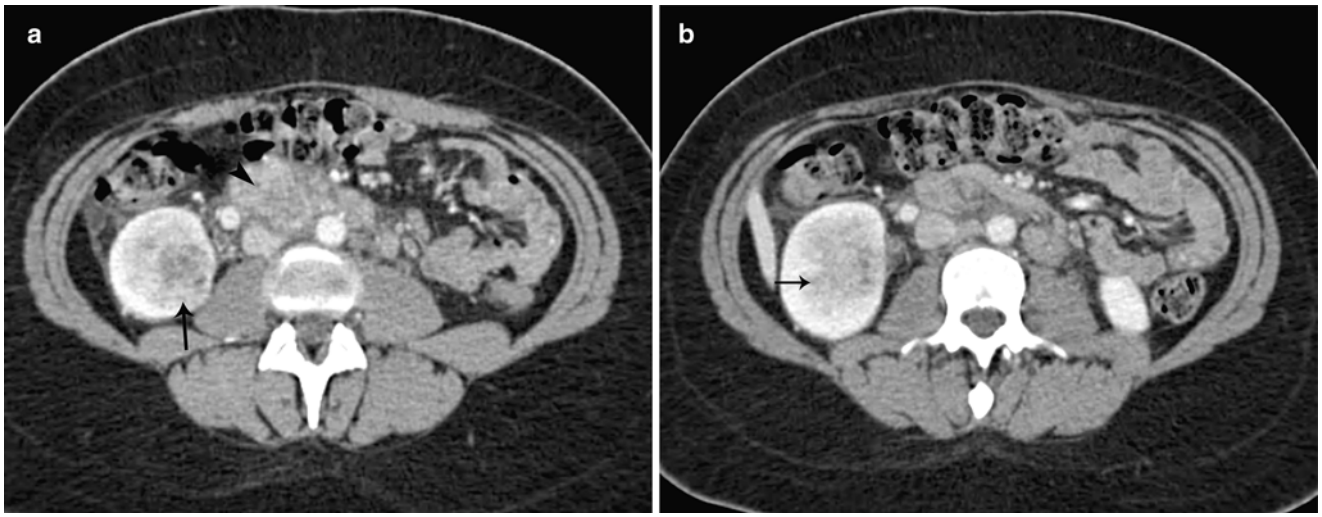

Fig. 10.23 Medullary carcinoma of kidney. (**a** and **b**) Axial contrast enhanced CT images from a 20-year-old girl with sickle cell trait show an infiltrative renal mass at the lower pole of the right kidney (*arrow*) with enlarged retroperitoneal lymph nodes (*arrowhead*)

Although the definitive cytogenetic characteristics of this neoplasm are yet to be established, the lesion is not known to demonstrate the common aberrations seen in other renal neoplasms, further supporting it as a separate entity. Cytogenetic studies of two neoplasms report monosomy 22 in both, duplication of the 7q32-36 region in one case, and multiple aberrations including monosomy 14, deletion at 3q11, and translocations at chromosomes 4 and 22 in the other [105]. Further studies are needed to support the significance of these findings.

Prognostic outlook for these patients is unclear. Partial or radical nephrectomy is used in most cases and usually clears any symptoms, with patients generally remaining recurrence free [107]. However, additional cases are needed to confirm this observation.

The imaging features of oncocytic PRCC following neuroblastoma have not been well described.

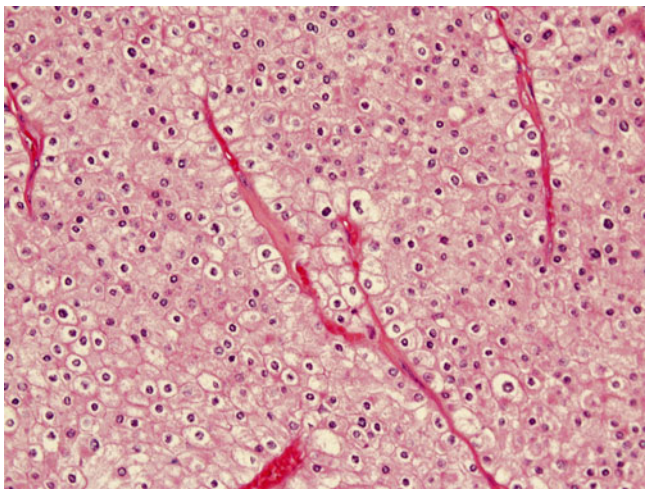

Fig. 10.24 Chromophobe renal cell carcinoma showing broad trabeculae with the tumor cells showing eosinophilic cells and some show vacuolated cytoplasm

Chromophobe RCC

Chromophobe renal cell carcinoma (CRCC) accounts for about 5 % of all renal cell carcinomas (RCC) and is extremely rare in childhood, with less than ten cases reported in the literature [108, 109]. The average age at diagnosis is during the fifth decade of life, and there is a slight predominance of females over males (52–48 %) [110]. Among the few pediatric cases the average age was 11.7 [108]. Most patients present asymptomatically, with the presence an abdominal mass, hematuria, or pain usually indicative of advanced disease. Generally metastasis is rare at presentation (6–7 % of cases) and the most common sites are the liver and lung [109].

Grossly, CRCC is usually larger than other RCC variants, with a median tumor size of 6 cm [109]. Additionally, lesions tend to be well-circumscribed and highly lobulated, and the cut surface tends to be brownish-tan. Microscopically, CRCC neoplasms present in two different histological variants: classic and eosinophilic. In the classic variant, cells are polygonal, pale and large, with abundant transparent cytoplasm. The eosinophilic variant has similar features to oncocytomas, which include a nested or alveolar architecture with granularity (Fig. 10.24). Additionally, there is a mixed variant in which neither of the two prominent variants occupies more than 80 % of the morphology. Also, some CRCC can show sarcomatoid changes, which are associated with more aggressive behavior and metastasis [111]. These lesions are characterized by positive Hale's colloidal iron staining in the cytoplasm.

The genetic features of CRCC are not fully understood. Chromosome losses at 2, 10, 13, 17, and 21 have been widely reported [109]. This variant does not show the 3p loss characteristic of nonpapillary RCCs [108]. Additionally, CRCC has been associated with Birt–Hogg–Dubé (BHD) syndrome, with over 30 % of patients with BHD presenting with CRCC. This familial syndrome is a result of inactivating mutations on the *FLCN* gene on the short arm of chromosome 17. Overall, CRCC has a good prognosis with about a 90 % survival rate at 10 years post diagnosis [112]. Interestingly, females appear to have much higher survival rates than males. Additionally, greater risk of mortality has been associated with high clinical or pathological stage and sarcomatoid differentiation [111].

The imaging features of chromophobe RCC have not been well described.

Primitive Neuroectodermal Tumors

Primitive neuroectodermal tumor (PNET) of the kidney belongs to a family of tumors that include Ewing sarcoma and Askin tumor, together comprising about 1 % of all sarcomas [113]. Specifically, PNET is a poorly differentiated neoplasm arising from the cells of the neuroectoderm that can occur anywhere in the soft tissues and rarely in the kidneys [114]. This neoplasm is malignant and must be differentiated from other round-cell tumors such as neuroblastoma and blastema-predominant Wilms' tumor.

Over 75 % of renal PNET cases occur between the ages of 10 and 39, with a median age of 24 years and a range from 4 to 66 years [115]. A slight male predominance has been reported in renal PNET but not confirmed, and it is more commonly reported among Hispanics and whites than in blacks and Asians [113]. Presenting symptoms vary and include abdominal pain, hematuria, malaise, fever, and dysuria [113, 114]. Over 50 % of these cases at presentation are a result of recurrence or metastasis [116].

Grossly, the tumors are solid and firm with necrosis and hemorrhage being commonly observed. Additionally, the lesion may be tan-yellow to gray-white in appearance and usually vary in size from about 8 to 16 cm in diameter [117]. Microscopically, most PNETs have typical features characterized by undifferentiated cells with round or ovoid hyperchromatic nuclei with minimal cytoplasm and mitotic figures [118]. Additionally, the most characteristic histological feature of PNET is the arrangement of cells forming pseudorosettes. There also exist PNETs with non-typical histology, which include those with CCSK-like, MPNST-like, rhabdoid, epithelioid, paraganglioma-like, and sclerosing morphologies [118]. Immunohistochemistry can be used to help in confirming PNET diagnosis. CD99 positivity is reported in the vast majority of lesions and further negative staining with WT-1 and CD45 can help to further separate PNET from Wilms' tumor and non-Hodgkin lymphoma respectively [113].

Over 85 % of PNET lesions show a genetic alteration with t(11;22)(q24;q12). This results in a chimeric fusion transcript of *EWS/FLI-1* gene products [119]. Additionally, about 5–10 % of PNET neoplasms have a t(21;22)(q22;q12) genetic mutation. These lesions follow a generally malignant clinical course with the majority of patients presenting with locally advanced disease and/or metastasis. The overall 5-year survival rate is reported to be between 45 and 55 % [115].

Imaging Features

Renal PNETs are large, heterogeneous tumors that may replace the entire kidney [120]. Presence of calcification, areas of internal hemorrhage or necrosis, and peripheral hypervascularity makes these tumors heterogeneous in appearance on all imaging modalities. On MR, PNETs demonstrate intermediate to high T2 signal intensity. They can show intravascular extension. Common sites of metastasis include lungs, bones, and liver.

Rhabdomyosarcoma of the Kidney

Primary rhabdomyosarcoma (RMS) of the kidney is extremely rare in the pediatric population, with fewer than ten cases reported in the literature [121]. Rhabdomyosarcomas can occur in the genitourinary tract or in the head and neck and have several histological subtypes, but only the conventional or embryonal type has been reported in pediatric renal cases [121]. Grossly, the lesions originate in the renal parenchyma and are poorly circumscribed and tan in appearance, with hemorrhage and necrosis common (Fig. 10.25). Microscopic features include cells separated by myxoid stroma with undifferentiated mesenchymal cells with ovoid

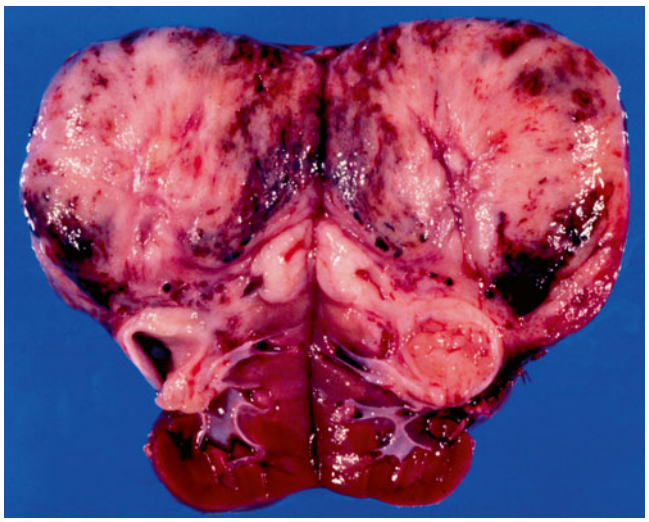

Fig. 10.25 Lesion occupying the upper pole of the renal parenchyma; it is poorly circumscribed and shows a tan cut surface, with hemorrhage and necrosis

nuclei and scant cytoplasm [122]. This tumor can be mistaken for blastemal predominant Wilms' tumor. Anaplasia was found in 67 % of cases reported in a study reviewing six renal RMS cases [121]. This prevalence greatly exceeds that of RMSs in general. Renal RMSs of the embryonal subtype are strongly immunopositive for desmin, myogenin, and MyoD1 (Fig. 10.26) [121]. Rhabdomyosarcoma of the kidney does not have any characteristic imaging findings, and the diagnosis has to be made at histopathological evaluation. It can present as a poorly enhancing, large soft tissue mass. Genetic mutations seen in embryonal RMS include LOH at 11p15.5, which is seen in Wilms' tumors and commonly associated with Beckwith–Wiedemann syndrome. Anaplasia usually carries the *PAX*/*FKHR* gene fusion. Of the cases reported, all but one were treated with radical nephrectomy. Survival rate is strongly diminished by metastasis at presentation with subsequent recurrence (survival years average: 6.5 (no metastasis or recurrence) vs. 1.1 (with) [121].

The imaging features of rhabdomyosarcoma of the kidney have not been well described.

Synovial Sarcoma

Primary renal synovial sarcoma (PRSS) is an extremely rare renal neoplasm with only about 65 cases reported in the literature in all age groups [123]. To our knowledge, two cases have been reported in the pediatric population with the youngest reported in a 13-year-old patient [124]. Generally, synovial sarcomas (SSs) account for about 10 % of all soft tissue sarcomas and can affect various regions of the body including the head and neck, bone, lung, and prostate [125]. Renal SS usually occurs in the adult population with a reported median age of 37 years [123]. Additionally, there appears to be no gender predominance. Patients often present with hematuria, flank/abdominal pain, and/or abdominal distention [126] with about 8 % demonstrating metastatic spread at diagnosis [123].

Grossly, the tumors are usually large, showing necrosis and containing cystic regions [126]. The lesions are described as tan in color and rubbery with hemorrhage and necrosis commonly observed. Microscopically, PRSS are made up of plump spindle cells with necrosis forming intersecting fascicles showing hyperchromatic nuclei [126]. Additionally, tumors cells at high power have a characteristic "rice grain" shape with minimal cytoplasm and frequent mitotic figures [126]. These lesions show immunopositivity most reliably for vimentin and bcl-2 [123].

The characteristic genetic mutation of PRSS is a translocation t(X;18)(p11;q11) resulting in an SSX-SYT gene fusion product thought to be implicated in transformation activity [123]. Two variants of the *SSX* gene (*SSX1* and *SSX2*) are most commonly implicated in PRSS with the *SSX2* variant occurring more often and also associated with a higher survival rate compared with *SSX1* [123]. Additionally, the *SSX4* variant has been rarely reported in PRSS [125]. Additionally, a translocation t(X;20)(p11;q13) has been associated with PRSS [127].

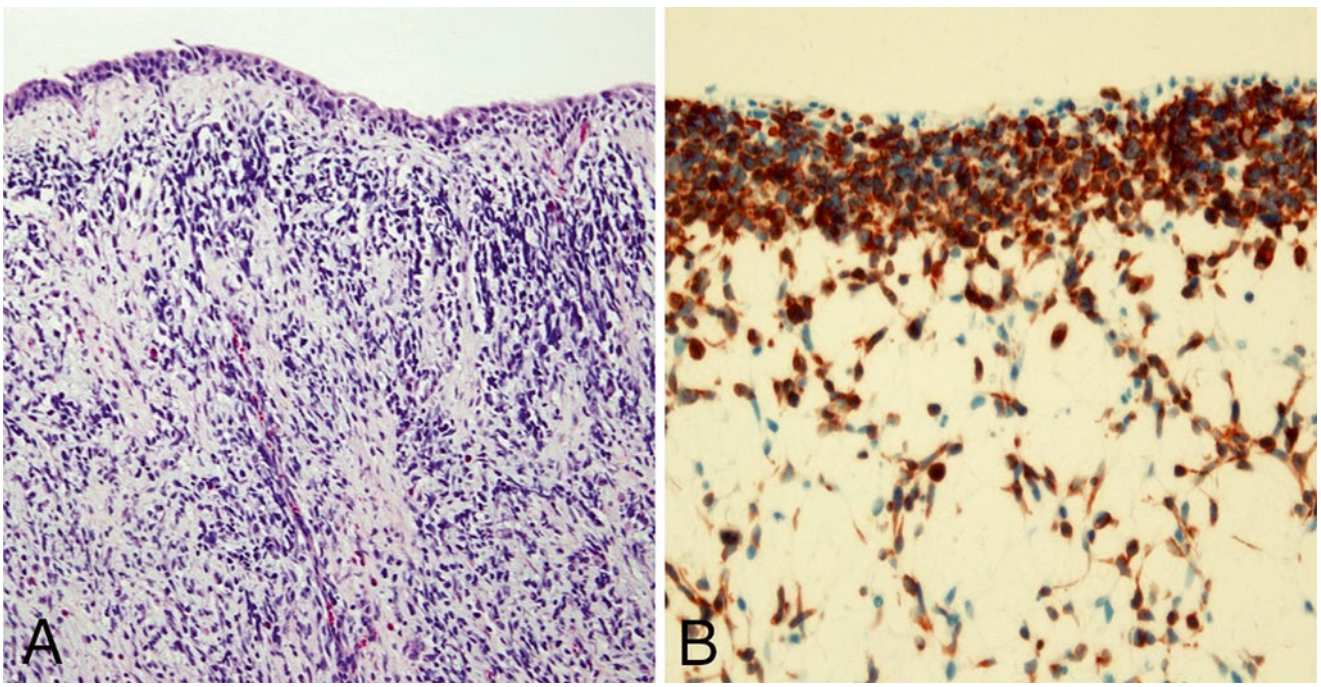

Fig. 10.26 Primary rhabdomyosarcoma of the kidney showing cambium layer (**a**) and strong positive desmin immunostain (**b**)

Synovial sarcomas in general have a poor prognostic outlook with a reported 36 % developing metastasis after nephrectomy [123]. Most common sites of metastasis include the lungs (42 %), abdominal lymph nodes and local recurrence (29 %), liver (24 %), and bone (6 %). Metastasis increases mortality with a median disease free survival of 33 months after diagnosis reported in non-metastatic patients and only 6 months for those developing metastatic disease [123].

Imaging Features

Renal synovial sarcoma appears as a large well-circumscribed heterogeneously enhancing soft-tissue mass that may extend into the renal pelvis or the perinephric region [128]. Some tumors may be predominantly cystic with enhancing septa and mural nodules. Extension into the renal vein and inferior vena cava has been described. At MR imaging, soft-tissue synovial sarcomas are heterogeneously hyperintense on T2-weighted images and hypointense on T1-weighted images with areas of hemorrhage, fluid levels, and septa [129].

References

1. Ko EY, Ritchey ML. Current management of Wilms' tumor in children. J Pediatr Urol. 2009;5(1):56–65.
2. Murphy WM, Grignon DJ, Perlman EJ. Kidney tumors in children. In: Silverberg SG, Sobin LH, editors. Tumors of the kidney, bladder, and related urinary structures. Washington, DC: American Registry of Pathology; 2004. p. 1–99.
3. Shen SS, et al. Recently described and emphasized entities of renal neoplasms. Arch Pathol Lab Med. 2007;131(8):1234–43.
4. Lall A, et al. Wilms' tumor with intracaval thrombus in the UK Children's Cancer Study Group UKW3 trial. J Pediatr Surg. 2006;41(2):382–7.
5. Servaes S, et al. Comparison of diagnostic performance of CT and MRI for abdominal staging of pediatric renal tumors: a report from the Children's Oncology Group. Pediatr Radiol. 2014 Aug 19. [Epub ahead of print].
6. Brisse HJ, et al. Imaging in unilateral Wilms tumour. Pediatr Radiol. 2008;38(1):18–29.
7. Charles AK, Vujanić GM, Berry PJ. Renal tumours of childhood. Histopathology. 1998;32(4):293–309.
8. Sebire NJ, Vujanic GM. Paediatric renal tumours: recent developments, new entities and pathological features. Histopathology. 2009;54(5):516–28.
9. Chu A, et al. Wilms' tumour: a systematic review of risk factors and meta-analysis. Paediatr Perinat Epidemiol. 2010;24(5):449–69.
10. Nakamura L, Ritchey M. Current management of wilms' tumor. Curr Urol Rep. 2010;11(1):58–65.
11. Davidoff AM. Wilms' tumor. Curr Opin Pediatr. 2009;21(3):357–64.
12. Keaney CM, Springate JE. Cancer and the kidney. Adolesc Med Clin. 2005;16(1):121–48.
13. Lowe LH, et al. Pediatric renal masses: Wilms tumor and beyond. Radiographics. 2000;20(6):1585–603.
14. Ritchey ML, et al. Renal vein involvement with nephroblastoma: a report of the National Wilms' Tumor Study-3. Eur Urol. 1990; 17(2):139–44.
15. Khanna G, et al. Evaluation of diagnostic performance of CT for detection of tumor thrombus in children with Wilms tumor: a report from the Children's Oncology Group. Pediatr Blood Cancer. 2012;58(4):551–5.
16. Khanna G, et al. Detection of preoperative Wilms tumor rupture with CT: a report from the Children's Oncology Group. Radiology. 2013;266(2):610–7.
17. Ehrlich PF. Bilateral Wilms' tumor: the need to improve outcomes. Expert Rev Anticancer Ther. 2009;9(7):963–73.
18. Rohrschneider WK, et al. US, CT and MR imaging characteristics of nephroblastomatosis. Pediatr Radiol. 1998;28(6):435–43.
19. Choueiri TK, et al. BRAF mutations in metanephric adenoma of the kidney. Eur Urol. 2012;62(5):917–22.
20. Schmelz HU, et al. Metanephric adenoma of the kidney: case report and review of the literature. Int Urol Nephrol. 2005;37(2): 213–7.
21. Davis Jr CJ, et al. Metanephric adenoma. Clinicopathological study of fifty patients. Am J Surg Pathol. 1995;19(10):1101–14.
22. Arroyo MR, et al. The spectrum of metanephric adenofibroma and related lesions: clinicopathologic study of 25 cases from the National Wilms Tumor Study Group Pathology Center. Am J Surg Pathol. 2001;25(4):433–44.
23. Hennigar RA, Beckwith JB. Nephrogenic adenofibroma. A novel kidney tumor of young people. Am J Surg Pathol. 1992;16(4): 325–34.
24. Hoglund HH, et al. Ossifying renal tumor of infancy (ORTI)—a rare diagnosis. Klin Padiatr. 2011;223(3):178–9.
25. Argani P, Beckwith JB. Metanephric stromal tumor: report of 31 cases of a distinctive pediatric renal neoplasm. Am J Surg Pathol. 2000;24(7):917–26.
26. Kacar A, et al. Metanephric stromal tumor: a challenging diagnostic entity in children. J Pediatr Surg. 2011;46(12):e7–10.
27. Grundy P, et al. Clinicopathologic correlates of loss of heterozygosity in Wilm's tumor: a preliminary analysis. Med Pediatr Oncol. 1996;27(5):429–33.
28. Argani P, Collins MH. Anaplastic nephrogenic rest. Am J Surg Pathol. 2006;30(10):1339–41.
29. Beckwith JB. Nephrogenic rests and the pathogenesis of Wilms tumor: developmental and clinical considerations. Am J Med Genet. 1998;79(4):268–73.
30. Lonergan GJ, et al. Nephrogenic rests, nephroblastomatosis, and associated lesions of the kidney. Radiographics. 1998;18(4): 947–68.
31. Beckwith JB. Precursor lesions of Wilms tumor: clinical and biological implications. Med Pediatr Oncol. 1993;21(3):158–68.
32. Beckwith JB, Kiviat NB, Bonadio JF. Nephrogenic rests, nephroblastomatosis, and the pathogenesis of Wilms' tumor. Pediatr Pathol. 1990;10(1–2):1–36.
33. Fukuzawa R, Reeve AE. Molecular pathology and epidemiology of nephrogenic rests and Wilms tumors. J Pediatr Hematol Oncol. 2007;29(9):589–94.
34. Charles AK, Brown KW, Berry PJ. Microdissecting the genetic events in nephrogenic rests and Wilms' tumor development. Am J Pathol. 1998;153(3):991–1000.
35. Hennigar RA, O'Shea PA, Grattan-Smith JD. Clinicopathologic features of nephrogenic rests and nephroblastomatosis. Adv Anat Pathol. 2001;8(5):276–89.
36. Park S, et al. Inactivation of WT1 in nephrogenic rests, genetic precursors to Wilms' tumour. Nat Genet. 1993;5(4):363–7.
37. Steenman M, et al. Comparative genomic hybridization analysis of Wilms tumors. Cytogenet Cell Genet. 1997;77(3–4):296–303.
38. Ritchey ML, et al. Fate of bilateral renal lesions missed on preoperative imaging: a report from the National Wilms Tumor Study Group. J Urol. 2005;174(4 Pt 2):1519–21. discussion 1521.
39. Gylys-Morin V, et al. Wilms tumor and nephroblastomatosis: imaging characteristics at gadolinium-enhanced MR imaging. Radiology. 1993;188(2):517–21.

40. Hausegger KA, et al. Can MR contribute to the diagnosis of nephroblastomatosis? A report of one case. Pediatr Radiol. 1991;21(7):533–5.
41. Perlman EJ, et al. Hyperplastic perilobar nephroblastomatosis: long-term survival of 52 patients. Pediatr Blood Cancer. 2006; 46(2):203–21.
42. Joshi VV, Beckwith JB. Multilocular cyst of the kidney (cystic nephroma) and cystic, partially differentiated nephroblastoma. Terminology and criteria for diagnosis. Cancer. 1989;64(2): 466–79.
43. Joshi VV, et al. Cystic partially differentiated nephroblastoma: a clinicopathologic entity in the spectrum of infantile renal neoplasia. Cancer. 1977;40(2):789–95.
44. Truong LD, et al. Renal cystic neoplasms and renal neoplasms associated with cystic renal diseases: pathogenetic and molecular links. Adv Anat Pathol. 2003;10(3):135–59.
45. Blakely ML, et al. Outcome of children with cystic partially differentiated nephroblastoma treated with or without chemotherapy. J Pediatr Surg. 2003;38(6):897–900.
46. Agrons GA, et al. Multilocular cystic renal tumor in children: radiologic-pathologic correlation. Radiographics. 1995;15(3): 653–69.
47. Bahubeshi A, et al. Germline DICER1 mutations and familial cystic nephroma. J Med Genet. 2010;47(12):863–6.
48. Bayindir P, et al. Cellular mesoblastic nephroma (infantile renal fibrosarcoma): institutional review of the clinical, diagnostic imaging, and pathologic features of a distinctive neoplasm of infancy. Pediatr Radiol. 2009;39(10):1066–74.
49. England RJ, et al. Mesoblastic nephroma: a report of the United Kingdom children's cancer and leukaemia group (CCLG). Pediatr Blood Cancer. 2011;56(5):744–8.
50. Furtwaengler R, et al. Mesoblastic nephroma—a report from the Gesellschaft fur Padiatrische Onkologie und Hamatologie (GPOH). Cancer. 2006;106(10):2275–83.
51. Gupta R, et al. Cellular mesoblastic nephroma in an infant: report of the cytologic diagnosis of a rare paediatric renal tumor. Diagn Cytopathol. 2009;37(5):377–80.
52. Chaudry G, et al. Imaging of congenital mesoblastic nephroma with pathological correlation. Pediatr Radiol. 2009;39(10):1080–6.
53. Irsutti M, et al. Mesoblastic nephroma: prenatal ultrasonographic and MRI features. Pediatr Radiol. 2000;30(3):147–50.
54. Portugal R, Barroca H. Clear cell sarcoma, cellular mesoblastic nephroma and metanephric adenoma: cytological features and differential diagnosis with Wilms tumour. Cytopathology. 2008; 19(2):80–5.
55. Rubin BP, et al. Congenital mesoblastic nephroma t(12;15) is associated with ETV6-NTRK3 gene fusion: cytogenetic and molecular relationship to congenital (infantile) fibrosarcoma. Am J Pathol. 1998;153(5):1451–8.
56. Henno S, et al. Cellular mesoblastic nephroma: morphologic, cytogenetic and molecular links with congenital fibrosarcoma. Pathol Res Pract. 2003;199(1):35–40.
57. Steelman C, et al. Unusual presentation of congenital infantile fibrosarcoma in seven infants with molecular-genetic analysis. Fetal Pediatr Pathol. 2011;30(5):329–37.
58. Brownlee NA, et al. Recurring translocation (10;17) and deletion (14q) in clear cell sarcoma of the kidney. Arch Pathol Lab Med. 2007;131(3):446–51.
59. Gooskens SL, et al. Clear cell sarcoma of the kidney: a review. Eur J Cancer. 2012;48(14):2219–26.
60. Argani P, et al. Clear cell sarcoma of the kidney: a review of 351 cases from the National Wilms Tumor Study Group Pathology Center. Am J Surg Pathol. 2000;24(1):4–18.
61. Cutcliffe C, et al. Clear cell sarcoma of the kidney: up-regulation of neural markers with activation of the sonic hedgehog and Akt pathways. Clin Cancer Res. 2005;11(22):7986–94.
62. Amin MB, et al. Clear cell sarcoma of kidney in an adolescent and in young adults: a report of four cases with ultrastructural, immunohistochemical, and DNA flow cytometric analysis. Am J Surg Pathol. 1999;23(12):1455–63.
63. Watts KE, Hansel DE, MacLennan GT. Clear cell sarcoma of the kidney. J Urol. 2011;185(1):279–80.
64. Glass RB, Davidson AJ, Fernbach SK. Clear cell sarcoma of the kidney: CT, sonographic, and pathologic correlation. Radiology. 1991;180(3):715–7.
65. O'Meara E, et al. Characterization of the chromosomal translocation t(10;17)(q22;p13) in clear cell sarcoma of kidney. J Pathol. 2012;227(1):72–80.
66. Schuster AE, et al. Genetic and genetic expression analyses of clear cell sarcoma of the kidney. Lab Invest. 2003;83(9):1293–9.
67. Desai SR, Upadhyay V. Rhabdoid tumour of the kidney: a diagnostic challenge and a fatal outcome. Pediatr Surg Int. 2000; 16(5–6):449–50.
68. Weeks DA, et al. Rhabdoid tumor of kidney. A report of 111 cases from the National Wilms' Tumor Study Pathology Center. Am J Surg Pathol. 1989;13(6):439–58.
69. Winger DI, et al. Radiology-Pathology Conference: rhabdoid tumor of the kidney. Clin Imaging. 2006;30(2):132–6.
70. Yamamoto M, et al. Treatment of stage IV malignant rhabdoid tumor of the kidney (MRTK) with ICE and VDCy: a case report. J Pediatr Hematol Oncol. 2006;28(5):286–9.
71. Han TI, et al. Rhabdoid tumour of the kidney: imaging findings. Pediatr Radiol. 2001;31(4):233–7.
72. Sisler CL, Siegel MJ. Malignant rhabdoid tumor of the kidney: radiologic features. Radiology. 1989;172(1):211–2.
73. Palmer NF, Sutow W. Clinical aspects of the rhabdoid tumor of the kidney: a report of the National Wilms' Tumor Study Group. Med Pediatr Oncol. 1983;11(4):242–5.
74. Nagata T, et al. Molecular genetic alterations and gene expression profile of a malignant rhabdoid tumor of the kidney. Cancer Genet Cytogenet. 2005;163(2):130–7.
75. Lee RS, et al. A remarkably simple genome underlies highly malignant pediatric rhabdoid cancers. J Clin Invest. 2012;122(8): 2983–8.
76. Gadd S, et al. Rhabdoid tumor: gene expression clues to pathogenesis and potential therapeutic targets. Lab Invest. 2010;90(5): 724–38.
77. Perlman EJ. Pediatric renal cell carcinoma. Surg Pathol Clin. 2010;3(3):641–51.
78. Sausville JE, et al. Pediatric renal cell carcinoma. J Pediatr Urol. 2009;5(4):308–14.
79. Soller MJ, et al. Cytogenetic findings in pediatric renal cell carcinoma. Cancer Genet Cytogenet. 2007;173(1):75–80.
80. Spreafico F, et al. Renal cell carcinoma in children and adolescents. Expert Rev Anticancer Ther. 2010;10(12):1967–78.
81. Indolfi P, et al. Local lymph node involvement in pediatric renal cell carcinoma: a report from the Italian TREP project. Pediatr Blood Cancer. 2008;51(4):475–8.
82. Selle B, et al. Population-based study of renal cell carcinoma in children in Germany, 1980–2005: more frequently localized tumors and underlying disorders compared with adult counterparts. Cancer. 2006;107(12):2906–14.
83. Argani P, et al. Primary renal neoplasms with the ASPL-TFE3 gene fusion of alveolar soft part sarcoma: a distinctive tumor entity previously included among renal cell carcinomas of children and adolescents. Am J Pathol. 2001;159(1):179–92.
84. Argani P, Ladanyi M. Translocation carcinomas of the kidney. Clin Lab Med. 2005;25(2):363–78.
85. Argani P, et al. A novel CLTC-TFE3 gene fusion in pediatric renal adenocarcinoma with t(X;17)(p11.2;q23). Oncogene. 2003;22(34): 5374–8.

86. Schafernak KT, et al. Pediatric renal cell carcinoma as second malignancy: reports of two cases and a review of the literature. Can J Urol. 2007;14(6):3739–44.
87. Joshi DD, Banerjee T. Vascular endothelial growth factor (VEGF) receptor antibody bevacizumab (avastin) induces regression of renal cell carcinoma in an adolescent resulting in residual tumorectomy. Pediatr Blood Cancer. 2008;50(4):903–4.
88. Malouf GG, et al. Targeted agents in metastatic Xp11 translocation/TFE3 gene fusion renal cell carcinoma (RCC): a report from the Juvenile RCC Network. Ann Oncol. 2010;21(9):1834–8.
89. Pwint TP, et al. An adult Xp11.2 translocation renal carcinoma showing response to treatment with sunitinib. Urol Oncol. 2011; 29(6):821–4.
90. Schultz TD, et al. Papillary renal cell carcinoma: report of a rare entity in childhood with review of the clinical management. J Pediatr Surg. 2011;46(6):e31–4.
91. Antonelli A, et al. Cytogenetic features, clinical significance and prognostic impact of type 1 and type 2 papillary renal cell carcinoma. Cancer Genet Cytogenet. 2010;199(2):128–33.
92. Delahunt B, Eble JN. Papillary renal cell carcinoma: a clinicopathologic and immunohistochemical study of 105 tumors. Mod Pathol. 1997;10(6):537–44.
93. Downey RT, et al. CT and MRI appearances and radiologic staging of pediatric renal cell carcinoma. Pediatr Radiol. 2012;42(4): 410–7. quiz 513–4.
94. Khanna G, et al. Cell carcinoma in children and adolescents: a summary of imaging findings from the Children's Oncology Group. Pediatr Radiol. 2014;44(Suppl):S136.
95. Coogan CL, et al. Renal medullary carcinoma in patients with sickle cell trait. Urology. 1998;51(6):1049–50.
96. Gangireddy V, et al. Response of metastatic renal medullary carcinoma to carboplatinum and Paclitaxel chemotherapy. Clin Genitourin Cancer. 2012;10(2):134–9.
97. Swartz MA, et al. Renal medullary carcinoma: clinical, pathologic, immunohistochemical, and genetic analysis with pathogenetic implications. Urology. 2002;60(6):1083–9.
98. Baig MA, et al. Renal medullary carcinoma. J Natl Med Assoc. 2006;98(7):1171–4.
99. Hakimi AA, et al. Renal medullary carcinoma: the Bronx experience. Urology. 2007;70(5):878–82.
100. Walsh AM, et al. Response to radiation in renal medullary carcinoma. Rare Tumors. 2011;3(3):e32.
101. Assad L, et al. Cytologic features of renal medullary carcinoma. Cancer. 2005;105(1):28–34.
102. Avery RA, et al. Renal medullary carcinoma: clinical and therapeutic aspects of a newly described tumor. Cancer. 1996;78(1):128–32.
103. Khan A, et al. Renal medullary carcinoma: sonographic, computed tomography, magnetic resonance and angiographic findings. Eur J Radiol. 2000;35(1):1–7.
104. Davidson AJ, et al. Renal medullary carcinoma associated with sickle cell trait: radiologic findings. Radiology. 1995;195(1):83–5.
105. Medeiros LJ, et al. Oncocytoid renal cell carcinoma after neuroblastoma: a report of four cases of a distinct clinicopathologic entity. Am J Surg Pathol. 1999;23(7):772–80.
106. Lack EE, Cassady JR, Sallan SE. Renal cell carcinoma in childhood and adolescence: a clinical and pathological study of 17 cases. J Urol. 1985;133(5):822–8.
107. Dhall D, et al. Pediatric renal cell carcinoma with oncocytoid features occurring in a child after chemotherapy for cardiac leiomyosarcoma. Urology. 2007;70(1):178e13–5.
108. Katzman PJ, Schwartz JI. Chromophobe renal cell carcinoma in a child: case report and review of the literature. Pediatr Dev Pathol. 2007;10(2):125–8.
109. Vera-Badillo FE, Conde E, Duran I. Chromophobe renal cell carcinoma: a review of an uncommon entity. Int J Urol. 2012;19(10):894–900.
110. Amin MB, et al. Chromophobe renal cell carcinoma: histomorphologic characteristics and evaluation of conventional pathologic prognostic parameters in 145 cases. Am J Surg Pathol. 2008; 32(12):1822–34.
111. Przybycin CG, et al. Chromophobe renal cell carcinoma: a clinicopathologic study of 203 tumors in 200 patients with primary resection at a single institution. Am J Surg Pathol. 2011;35(7): 962–70.
112. Volpe A, et al. Chromophobe renal cell carcinoma (RCC): oncological outcomes and prognostic factors in a large multicentre series. BJU Int. 2012;110(1):76–83.
113. Bartholow T, Parwani A. Renal primitive neuroectodermal tumors. Arch Pathol Lab Med. 2012;136(6):686–90.
114. Chu WC, et al. Primitive neuroectodermal tumour (PNET) of the kidney: a rare renal tumour in adolescents with seemingly characteristic radiological features. Pediatr Radiol. 2008;38(10): 1089–94.
115. Ellinger J, et al. Primitive neuroectodermal tumor: rare, highly aggressive differential diagnosis in urologic malignancies. Urology. 2006;68(2):257–62.
116. Gonlusen G, et al. Primitive neuroectodermal tumor of the kidney: a rare entity. Int Urol Nephrol. 2001;33(3):449–51.
117. Jimenez RE, et al. Primary Ewing's sarcoma/primitive neuroectodermal tumor of the kidney: a clinicopathologic and immunohistochemical analysis of 11 cases. Am J Surg Pathol. 2002;26(3):320–7.
118. Parham DM, et al. Primary malignant neuroepithelial tumors of the kidney: a clinicopathologic analysis of 146 adult and pediatric cases from the National Wilms' Tumor Study Group Pathology Center. Am J Surg Pathol. 2001;25(2):133–46.
119. de Alava E, Gerald WL. Molecular biology of the Ewing's sarcoma/primitive neuroectodermal tumor family. J Clin Oncol. 2000;18(1):204–13.
120. Kim MS, et al. Radiologic findings of peripheral primitive neuroectodermal tumor arising in the retroperitoneum. AJR Am J Roentgenol. 2006;186(4):1125–32.
121. Raney B, et al. Primary renal sarcomas in the Intergroup Rhabdomyosarcoma Study Group (IRSG) experience, 1972–2005: a report from the Children's Oncology Group. Pediatr Blood Cancer. 2008;51(3):339–43.
122. Putnam AR, Wallentine JC. Diagnostic pathology. Pediatric neoplasms. 1st ed. Salt Lake City, UT: Amirsys; 2012.
123. Iacovelli R, et al. Clinical and pathological features of primary renal synovial sarcoma: analysis of 64 cases from 11 years of medical literature. BJU Int. 2012;110(10):1449–54.
124. Scarpato KR, et al. Primary renal synovial sarcoma in a 13-year-old boy. J Pediatr Surg. 2011;46(9):1849–51.
125. Divetia M, et al. Synovial sarcoma of the kidney. Ann Diagn Pathol. 2008;12(5):333–9.
126. Argani P, et al. Primary renal synovial sarcoma: molecular and morphologic delineation of an entity previously included among embryonal sarcomas of the kidney. Am J Surg Pathol. 2000;24(8):1087–96.
127. Fisher C. Diagnostic pathology. Soft tissue tumors. Salt Lake City, UT: Amirsys; 2011.
128. Perlmutter AE, et al. Primary synovial sarcoma of the kidney. Int J Urol. 2005;12(8):760–2.
129. Zakhary MM, et al. Magnetic resonance imaging features of renal synovial sarcoma: a case report. Cancer Imaging. 2008; 8:45–7.